ORNL/TM-2002/254

MEASUREMENTS OF WATER AND B_4C CONTENT OF RACKABLE CAN STORAGE BOXES FOR HEU STORAGE AT THE HEUMF AT THE Y-12 NATIONAL SECURITY COMPLEX

J. S. Neal, S. A. Pozzi, J. D. Edwards, and J. T. Mihalczo

December 2002

Prepared by
OAK RIDGE NATIONAL LABORATORY
P. O. Box 2008
Oak Ridge, Tennessee 37831
managed by
UT-Battelle, LLC
for the
U.S. DEPARTMENT OF ENERGY
under contract DE-AC05-00OR22725

CONTENTS

CONTENTS (cont'd.)

LIST OF FIGURES

LIST OF FIGURES (cont'd.)

Figure **Page**

LIST OF FIGURES (cont'd.)

LIST OF FIGURES (cont'd.)

LIST OF TABLES

LIST OF TABLES (cont'd.)

ABSTRACT

Extensive measurements at the Oak Ridge National Laboratory (ORNL) with BoroBond™ blocks of varying thickness, natural boron carbide (B_4C) content, and water content, and with a simplified mockup of the Rackable Can Storage Box (RCSB) of fixed natural B_4C and water content, have led to a method of quantifying the water content of RCSBs by fast neutron time-of-flight transmission measurements (NMIS)* and quantifying the B_4C content with gamma ray spectrometry assuming the water content is known. The time-of-flight transmission measurements results can also be used to assess the uniformity of the BoroBond™ in the RCSB. The data from both measurements will be stored for future comparisons to initial measurements. These methods can also be implemented at the RCSB production site, or subsequently at the Y-12 National Security Complex during the operating lifetime of the RCSBs at the Highly Enriched Uranium Materials Facility.

* The time-of-flight transmission measurements utilized the Nuclear Materials Identification System (NMIS) with ^{252}Cf source. NMIS is the system for confirmation of receipts and inventories at HEUMF.

1. INTRODUCTION

BoroBond™, which is a ceramic material containing natural boron carbide (neutron absorber) and water (neutron attenuator), is the filler material of the Rackable Can Storage Boxes (RCSBs) that will store highly enriched uranium in cans at the Highly Enriched Uranium Materials Facility (HEUMF) at the Y-12 National Security Complex. Both attenuation and absorption are essential for nuclear criticality safety of the fissile material stored in RCSBs. Some details of the mockup RCSB are given in Appendix A where the BoroBond™ material is also described. This BoroBond™ material has not yet been used for storage of HEU. To characterize the neutron attenuation and neutron absorption properties of this material, the Oak Ridge National Laboratory (ORNL) has performed an extensive series of measurements which included: fast neutron and gamma time-of-flight transmission using the Nuclear Materials Identification System (NMIS), thermal and epithermal neutron counting with ^{3}He proportional counters, and activation analysis with gamma ray spectrometry using a high purity germanium (HPGe) detector. These measurements were performed for a series of 12x12-in. square blocks of thickness varying from 2 to 12 in., with nominal[†] natural B_4C contents of 0, 2.3, 4.6, and 9.1 wt%, and two water contents achieved by baking the blocks to remove approximately 5/6 of the water. The measured dimensions and weights of these blocks are given in Appendix B. These measurements were also performed with a special RCSB of BoroBond™ material with nominal 4.6% natural B_4C. The chemical analysis of the material is not yet available and some limited information is given in Appendix A. All three measurement methods used ^{252}Cf sources.

The purpose of this work was to develop methods for quantification of the water and B_4C content of the RCSBs at the production site, upon receipt at Y-12, or at any time of their useful life in the HEUMF. Another purpose was to provide data that can be used to verify Monte Carlo neutron transport theory methods that are used for criticality safety analysis. The latter is important since this material has never been used for an isolating material in a highly enriched uranium metal storage facility.

This report describes the measurement methods, the configuration of the sources, detectors, and materials, the data obtained from some of the measurements, the analysis of the data, and recommendations for quantification of both the water and B_4C content of the RCSBs. The details of the ^{252}Cf sources are given in Appendix C. Not all of the approximately 900 measurements (~400 gamma ray spectrometry, ~400 fast neutron time-of-flight transmission with NMIS, and ~100 neutron counting measurements) that were performed are presented in this report, because many were exploratory investigations to determine how to best perform the measurements. A photograph of the special mockup of a RCSB is given in Appendix A. The special RCSB used in the measurements did not have steel on top and the top of the BoroBond™ was exposed to air.

[†] As yet, we do not have the analysis results from the manufacturer. As a result, no benchmarking calculations have been performed to date.

2. NEUTRON TIME-OF-FLIGHT TRANSMISSION MEASUREMENTS

The isolation properties of BoroBond™ depend mainly on the water content much in the same way as the water in the concrete of present storage vaults at the Y-12 National Security Complex isolates one can of highly enriched uranium (HEU) from another. In the RCSBs, the neutrons are slowed down to lower energy mainly by scattering with the hydrogen of the water in the BoroBond™. Fast neutron transmission should depend strongly on water content. The ^{252}Cf source for these measurements was electroplated on one plate of a parallel plate ionization chamber that produces an electrical timing pulse each time ^{252}Cf spontaneously fissions (sketch in Appendix C, Fig. C1). All results are presented in units of counts per single Cf fission, which emits an average of 3.73 prompt neutrons and 7.8 gamma rays per fission. The fission neutrons from ^{252}Cf have an energy distribution similar to that for uranium fission but slightly higher in energy. The emitted fission gamma rays and fast neutrons enter the BoroBond™ blocks, and their transmission was measured by proton recoil scintillation detectors on the opposite side from the source as a function of time after Cf fission with the NMIS processor. Measurements were performed for the blocks of varying thickness, B_4C, and water content, and for the RCSB. Measurements were performed with plastic scintillation detectors and some very limited exploratory measurements with liquid scintillation detectors.

2.1 DETECTION EFFICIENCY MEASUREMENTS

In order to use these data for verification of Monte Carlo transport theory methods, the efficiency of the detector as a function of neutron energy must be known. For these measurements, the detector was located 1 meter from the Cf source and a time-of-flight measurement in air was performed (5 minutes measurement time). Knowing the solid angle subtended by the detector, the distance between the source and detector, the energy spectrum of fission neutrons from ^{252}Cf, the number of neutrons per ^{252}Cf fission, and the measured counts per ^{252}Cf fission as a function of time after fission, the neutron detection efficiency per incident neutron as a function of energy can be obtained. At the beginning of each day of measurements, the time-of-flight distribution in air was measured for a 1 meter separation between the detector and the Cf source. At various times during the measurements with the blocks, this type of measurement was repeated with a source detector separation distance of 13.5 in., which was the spacing between the source and detector in the time-of-flight transmission measurements with the blocks.

2.2 PLASTIC SCINTILLATION DETECTOR EFFICIENCY

This detector was a 3.75x3.75x4.0-in.-thick plastic Bicron BC420 scintillation detector encased in a light-tight aluminum casing without Pb shielding.[‡] The measured time-of-flight distribution for the 1 meter distance is shown in Fig. 2.2.1. The initial peak is the gamma rays from the ^{252}Cf fission, which arrive at the detector first. The following broader distribution is the neutron distribution from Cf fission, with the faster neutrons arriving at earlier times. The detection efficiency as a function of neutron energy is shown in Fig. 2.2.2,

[‡] In conventional NMIS measurements with fissile material 6.3-mm-thick lead surrounds the scintillator. In these measurements since there was no significant background radiation, no shielding was used.

where it has a maximum value of 70% at about 1.5 MeV, and a threshold of about 0.5 MeV. Above the threshold the efficiency increases and after about 1.5 MeV it decreases due to the decreasing value of the hydrogen cross section with energy. The efficiency is the probability of detection for a neutron incident on the front face of the detector.

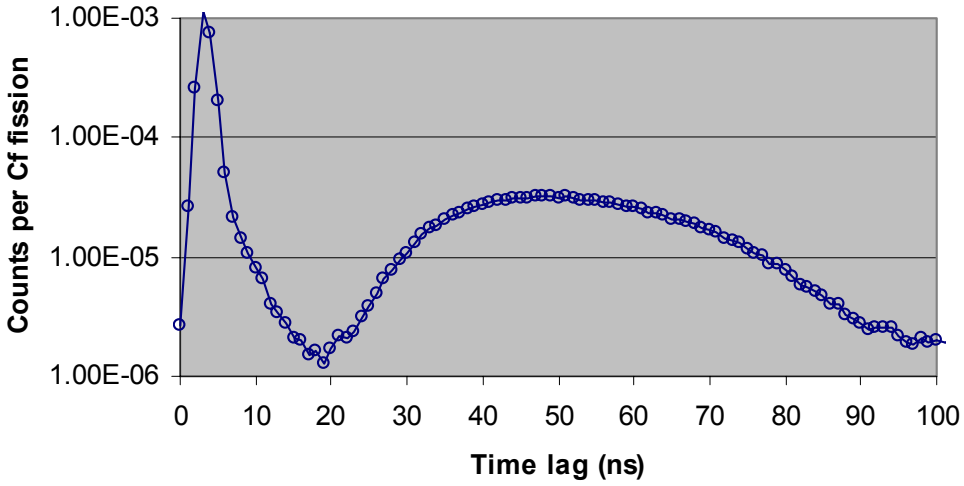

Fig. 2.2.1. Measured time-of-flight distribution for source-plastic scintillation detector (3.75 × 3.75 × 4.0-in.-thick) at a distance of 1 m.

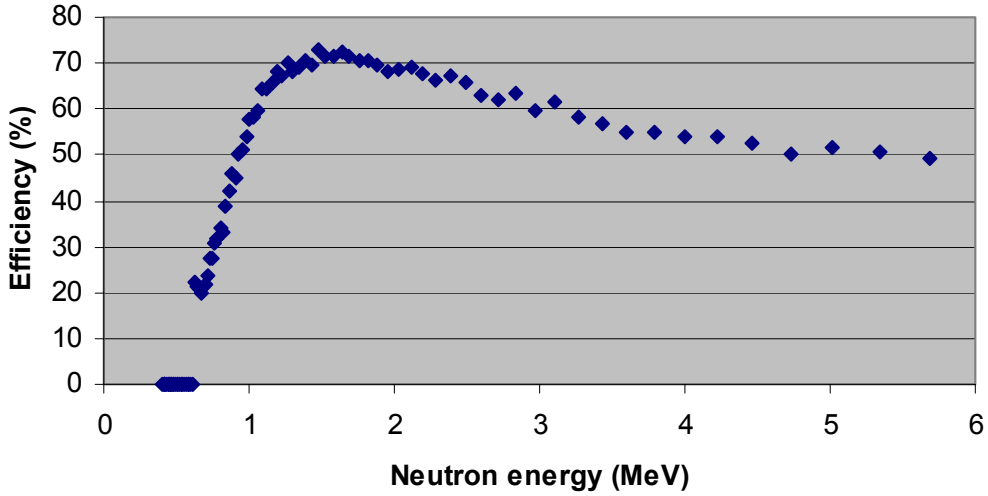

Fig. 2.2.2. Neutron detection efficiency for a 3.75 x 3.75 x 4.0-in.-thick plastic scintillator obtained from the source-detector time-of-flight distribution at 1 m of Fig. 2.2.1.

The measured time-of-flight distribution for the spacing of 13.5 in is given in Fig. 2.2.3, and the detection efficiency obtained from it given in Fig. 2.2.4. The 13.5 in. is the separation of the source and the detector in the BoroBond™ block measurements, and was

performed periodically with the blocks removed. The peak detection efficiency of 64% is lower than that measured at 1 meter due to dependence of path lengths through the detector on distance between the source and detector. For larger distances, the neutrons from the ^{252}Cf source are more parallel to the line between the center of the source and the detector, and enter the detector more perpendicular to its front face. Thus, they have longer path lengths in the detector. At the shorter distance 13.5 in., the shorter path length at the outer edges of the detector reduce the efficiency slightly. This effect is well known and has been observed previously. These measurements were repeated during the neutron time-of-flight transmission measurements with the blocks to confirm the stability of the measurement system.

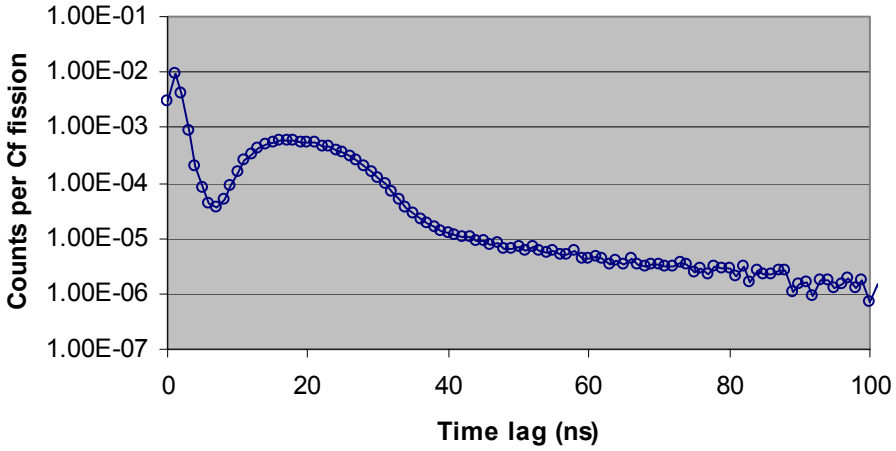

Fig. 2.2.3. Measured time-of-flight distribution for the 3.75 x 3.75 x 4.0-in.-thick plastic scintillator at a source-detector distance of 13.5 in.

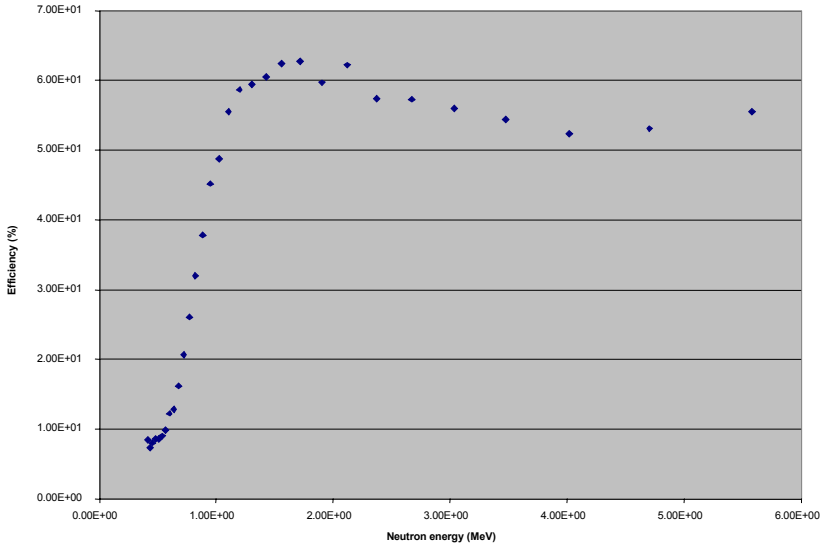

Fig. 2.2.4. Neutron detection efficiency for a 3.75x3.75x4.0-in.-thick plastic scintillator obtained from the source-detector time-of-flight distribution at 13.5 in. of Fig. 2.2.3.

2.3 BLOCK MEASUREMENTS WITH PLASTIC SCINTILLATORS

A photograph of the measurement setup for the blocks is shown in Fig. 2.3.1. The source is underneath the 4-in.-thick BoroBond™ block, which has a base with dimensions 12-in. by 12-in. The block rests on a 0.125-in.-thick carbon steel platform of a lift, which was 47.5 in. above the concrete floor. A 1.25-in.-diam hole in the carbon steel allowed the ^{252}Cf source ionization chamber to be in contact with the lowest block of a configuration. A 3.75x3.75x4.0-in.-thick plastic scintillation detector was mounted 13.5 in. above the source. For all measurements, the bottom of the blocks was 47.5 in. above the floor with front face of the detector 61 in. above the floor. The source and detector were aligned with the center of the block. The source-detector distance was not varied for different block thicknesses and this geometry was typical of a time-of-flight transmission measurement through the block. The detector height allowed a stack of three blocks.

Fig. 2.3.1. Photograph of measurement setup for fast plastic scintillator fast neutron time-of-flight transmission measurements.

Fig. 2.3.2 shows an example of a 270 sec measurement result for the transmission measurement with block A1* and with no block. The counts per Cf fission as a function of detection time following Cf fission are plotted. The ^{252}Cf fission rate was 9.7×10^5 per sec so approximately 7×10^4 counts were collected each time lag near the peak of the distribution. The first particles to arrive at the detector are the prompt gamma rays from fission, followed by directly transmitted fast neutrons, and then by neutrons that have scattered. The neutron detection threshold was approximately 0.5 MeV.

* Blocks designated A, B, C, and D had nominal B_4C contents of 0, 2.3, 4.6, and 9.1%, respectively. Blocks 4-in-thick were designated by numbers 1, 2, 3, and 4, and 2-in-thick blocks were designated by numbers 5, 6, 7, and 8. Only even numbered blocks were baked. Thus A1 designates a 4-in.-thick block with no B_4C content.

The analysis of the measurement results relies on the selection of features from the cross-correlation functions that are sensitive to the quantity of interest. The transmission measurements had the aim of determining the water content of the blocks. A number of features were analyzed, and the feature most sensitive to water content turned out to be the integral of the neutron peak for time lags corresponding to neutron energies from 0.5 to 2 MeV. Because the hydrogen cross section decreases at higher energy, this response was more sensitive than that for higher energy neutrons. The measurements performed are listed in Table 2.3.1, together with the integrals of the neutron distribution per Cf fission for the interval 0.5 to 2.0 MeV.

Not all the data are given in Table 2.3.1. Other measurements were performed at some of the same thicknesses as Table 2.3.1, for different combination of blocks. For example, there were measurements with blocks 7 and 8 that were also 2-in.-thick, 4 combinations of blocks that were 4-in.-thick, and other combinations that were 6-in.-thick. The measurement times were such that ~10^5 coincident counts or more were collected at a single time lag at the peak of the neutron distribution.

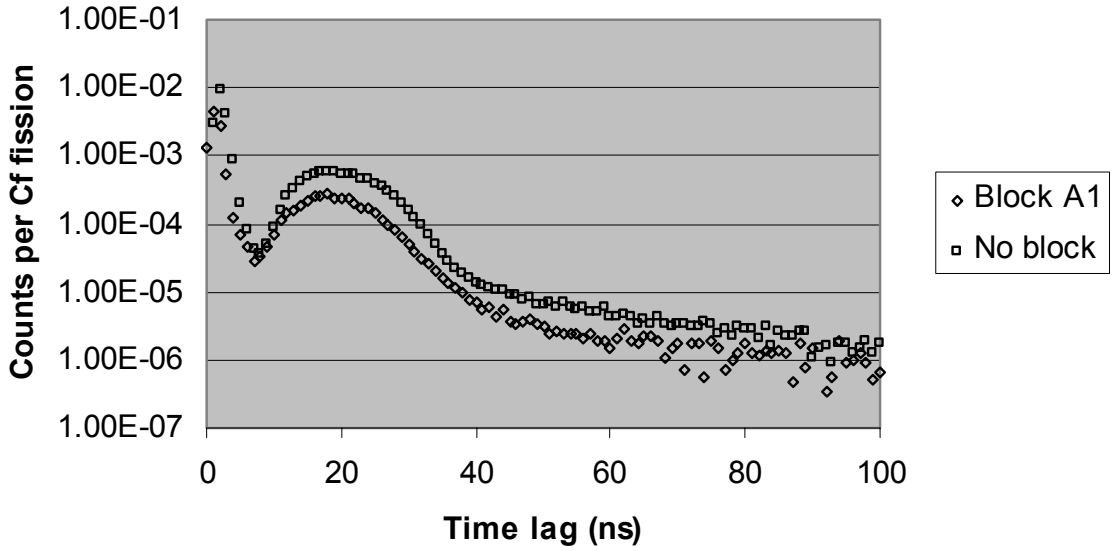

Fig. 2.3.2. Time-of-flight transmission measurement with the plastic scintillator results for no block and block A1 between the source and detector. The measurement time was ~256 seconds with a source of 9.7×10^5 fissions per second.

Table 2.3.1. Integral of the fast neutron transmission distributions between 0.5 and 2 MeV for measurements with the plastic scintillation detector for BoroBond™ blocks with B_4C contents of 0, 2.3, 4.6, and 9.1 wt%

Thickness* (inches)	Block numbers**	Integral per ^{252}Cf Fission for blocks of varying B_4C content***			
		A	B	C	D
2	5	2.65E-03	2.57E-03	2.61E-03	2.60E-03
2	6	3.33E-03	3.32E-03	3.35E-03	3.36E-03
4	1	1.68E-03	1.68E-03	1.69E-03	1.63E-03
4	2	2.77E-03	2.72E-03	2.77E-03	2.72E-03
6	1, 5	8.85E-04	8.79E-04	8.96E-04	8.51E-04
6	2, 6	1.94E-03	1.93E-03	1.99E-03	1.91E-03
8	1, 3	5.38E-04	5.66E-04	5.55E-04	5.15E-04
8	2, 4	1.55E-03	1.52E-03	1.56E-03	1.48E-03
10	1, 3, 5	3.80E-04	3.89E-04	3.82E-04	3.54E-04
10	2, 4, 6	1.39E-03	1.34E-03	1.37E-03	1.29E-03
12	1, 3, 5, 7	2.31E-04	2.36E-04	2.36E-04	2.17E-04
12	2, 4, 6, 8	1.14E-03	1.10E-03	1.10E-03	1.04E-03

*The measurement times were 4.4 min. for thicknesses of 2 and 4-in., 9 min. for thicknesses of 6 and 8-in., 18 min. for thickness of 10-in., and 45 min. for the 12-in. thickness.

**Even-numbered blocks were baked to remove 5/6 of the water. Four-inch thick blocks were numbered 1 to 4 and 2-in. thick blocks were numbered 5 to 8. Block numbers in the measurements are listed from the bottom up, the first adjacent to the source and the last closest to the detector.

***Nominal wt% B_4C is 0, 2.3, 4.6, and 9.1 wt% for the A, B, C, and D blocks respectively.

The time-of-flight distributions per Cf fission for the unbaked C series blocks of varying thicknesses are given in Fig. 2.3.3. Not all the data can be shown but some integral quantities can be plotted as a function of thickness for various B_4C contents. The integral of the neutron distribution (for neutron energy 0.5 to 2 MeV) as a function of thickness is plotted in Fig. 2.3.4. As it can be seen, this integral depends very slightly, if at all, on B_4C content, but does depend on the water content. In the measurements, two sets of blocks were available: an 'unbaked' set with full water content, and a 'baked' set, with approximately 5/6 of the water content removed. The ratio of the neutron integral for the 'baked' and 'unbaked' measurements is a factor of 3, approximately, for block thickness equal to 8 in., and almost 3.6 for 10-in.-thick C blocks, which have 4.6 wt% B_4C. These are approximately the thicknesses between adjacent holes in the RCSB (9 and 11 in.). These differences decrease with block thickness as expected.

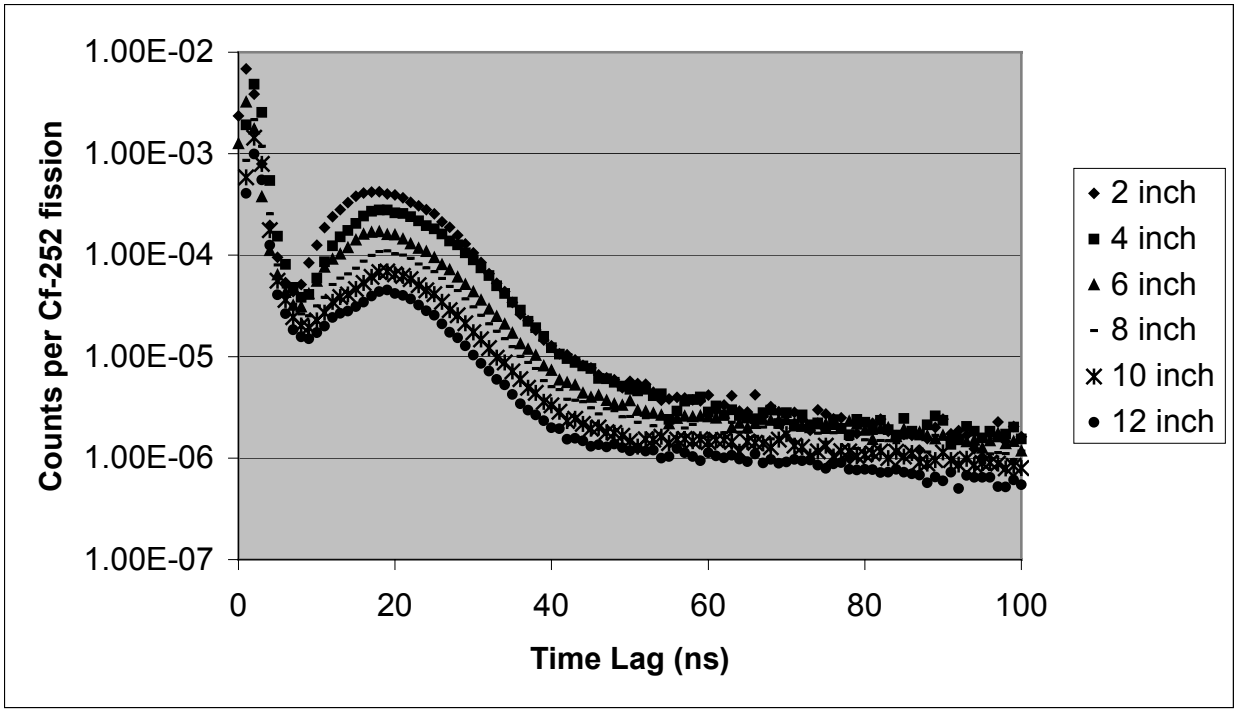

Fig. 2.3.3. Time-of-flight transmission measurement with the plastic scintillator for unbaked C blocks as a function of thickness.

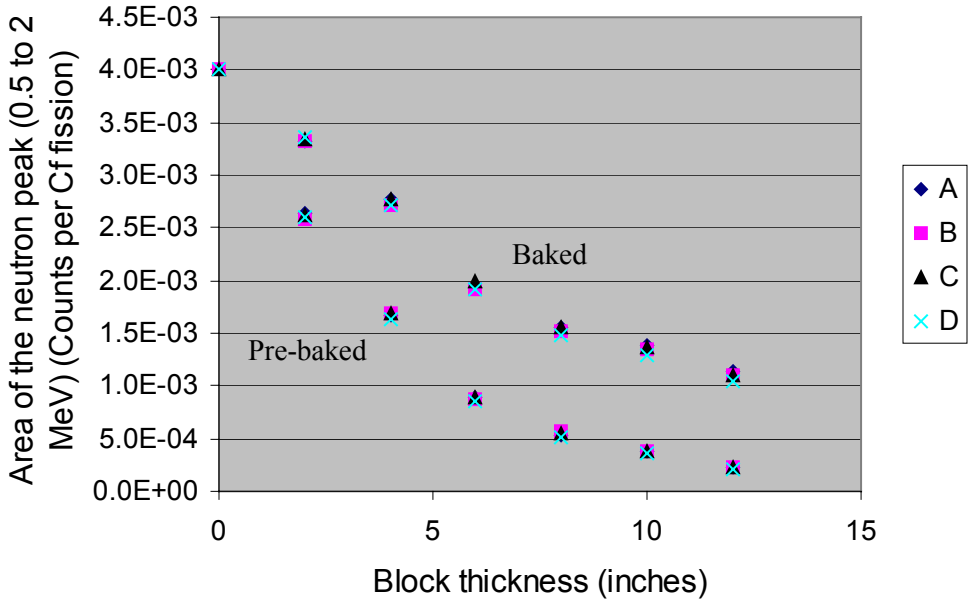

Fig. 2.3.4. Area of the neutron distribution for neutron energy 0.5 to 2 MeV as a function of block thickness for the plastic scintillator.

2.4 MEASUREMENTS WITH THE RCSB

Fast neutron time-of-flight transmission measurements were performed for the mockup RCSB with two different source locations. The first is shown in Fig. 2.4.1, which is a photograph of the mockup RCSB with a source in one fissile storage location and a plastic scintillation detector in another. The mockup RCSB was oriented vertically to minimize floor reflection effects. In actual verification measurements, the RCSB will be located horizontal about 3 feet off the floor, and floor effects will be corrected. The fissile storage locations were numbered 1 to 6 starting at the upper right of this photo 1, 2, 3 across the top right to left and 4, 5, 6 across the bottom left to right. For these measurements, the source was located in the center of fissile location 1 and the detector sequentially in locations 2, 3, 4, 5, and 6, and source also in location 2 with the detectors in locations 1, 3, 4, 5, and 6. Typical transmission measurement distributions between hole and the other 5 locations with detectors are shown in Fig. 2.4.2.

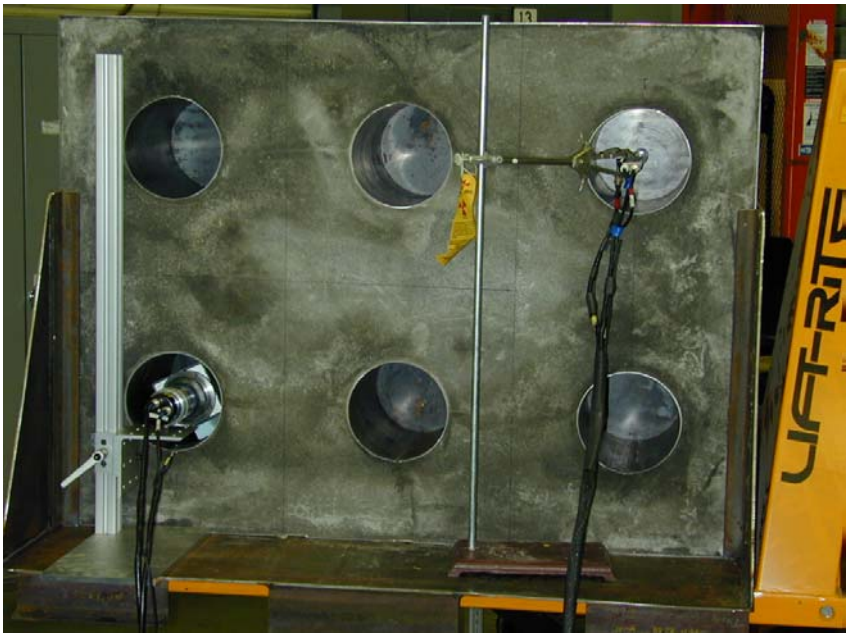

Fig. 2.4.1. Photograph of the mockup RCSB with the Cf source in fissile location 1 and the detector in fissile location 4.

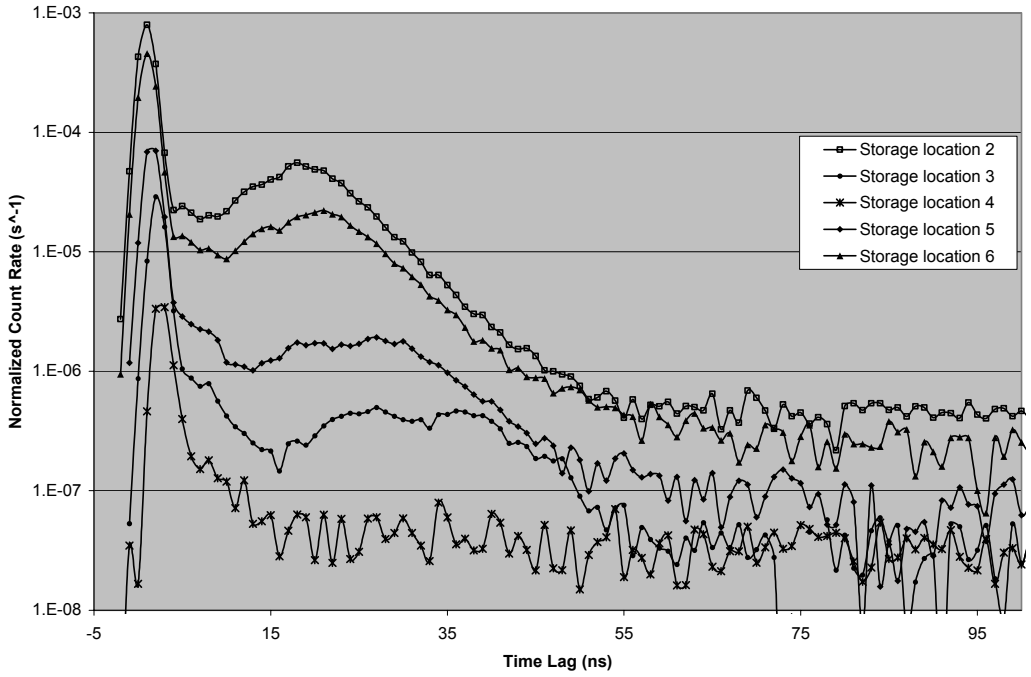

Fig. 2.4.2. Time-of-flight transmission measurement results for the source in hole 1 and the detector in holes 2 to 6.

Integrals of the neutron peak of the transmission measurements are given in Table 2.4.1. The table also shows the integrals for the measurements performed with the source in hole 2, and the detector in locations 1, 3, 4, 5, and 6. These integrals are related to the product of the detection efficiency and the number of neutrons per fission transmitted between fissile storage locations in the RCSB. Fission neutron attenuation is larger with greater spacing between holes. For non-adjacent holes the attenuation is an order of magnitude higher than for adjacent holes. These low transmissions reflect the good fast neutron isolation properties of BoroBond™ of these thicknesses.

Table 2.4.1. Integral of neutron peak per Cf fission for mockup RCSB transmission measurements with source in fissile storage locations 1 and 2[a]

Source position	Integral of neutron peak for detector in fissile storage locations					
	1	2	3	4	5	6
1	--	8.17E-04	1.65E-05	4.83E-06	5.14E-05	3.82E-04
2	8.50E-04	--	8.27E-04	5.46E-05	4.20E-04	5.21E-05

[a]Numbers in this table refer to fissile storage locations.

Another series of measurements was performed with different source-detector locations. In this configuration, the ^{252}Cf source was placed in a different location, as shown in the photograph of Fig. 2.4.3. Two 1-in.-diam and 6-in.-deep source holes were drilled in the RCSB. The one on the left is designated source hole A, and the one on the right as source hole B. These source holes were each equidistant between four fissile storage locations.

This geometry is that recommended for the at-the-factory verifications. These source holes would be provided in each RCSB. Sources in these holes will provide unambiguous repeatable location of the sources for this type of measurement, provide a storage location for the sources when not in use at the factory for verification, and, because of symmetry of the source-detector locations, indicate the uniformity of the BoroBond™ of the RCSB. Because of symmetry, responses B1, B6, A3, A4 and B2, B5, A2, A5 should be alike. The results of these measurements are given in Table 2.4.2.

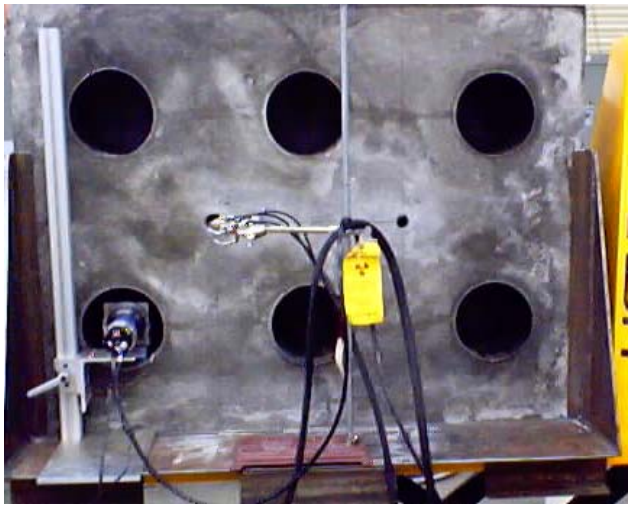

Fig. 2.4.3. Photograph of measurement setup for the mockup RCSB transmission measurements with Cf source located in hole A and detector in fissile storage location 4.

Table 2.4.2. Integral of neutron peak per Cf fission for the mockup RCSB transmission measurements with source in holes A and B[a]

Source position	Integral of neutron peak for detector in fissile storage locations					
	1	2	3	4	5	6
A	--	3.10E-03	3.11E-03	3.50E-03	3.46E-03	--
B	2.83E-03	2.94E-03	--	--	3.81E-03	3.61E-03

[a] Numbers in this table refer to fissile storage locations.

The values of Table 2.4.2 are higher than those of the previous configuration (Table 2.4.1) because there is less material between the source and the detector. The increased response of the detectors in the lower fissile storage locations is the result of floor reflection and can be corrected for. However, the response A3 is 10% higher than B1 and in A2 is slightly higher than B2. These may indicate some slight non-uniformity of BoroBond™ in the mockup RCSB. Even with these differences, the low transmissions indicate the good neutron isolation properties of BoroBond™ at these thicknesses.

2.5 DETERMINATION OF HYDROGEN CONTENT

A number of simulations were performed with the Monte Carlo code MCNP-PoliMi for blocks of varying water content.[§] Figure 2.5.1 shows the result of these simulations for neutron transmission measurements for the 8-in.-thick blocks. The experimental curves for the "baked" and "unbaked" blocks are also shown (corresponding to 17% and 100% water, respectively).

As expected, attenuation of the neutrons from the source increases with water content. A feature was extracted from the transmission measurements to be related to the water content of the blocks. The feature is the total integral of the counts in the neutron peak. Fig. 2.5.2 shows the value of this feature as a function of water content. The Monte Carlo calculational results were fit to an exponential function of water content. The results of the measurements are also shown in Fig 2.5.2. As it can be seen, there is good agreement between the Monte Carlo simulation and the measurements. These Monte Carlo calculations used nominal atomic compositions and not those from analysis (not yet received from Eagle Picher).

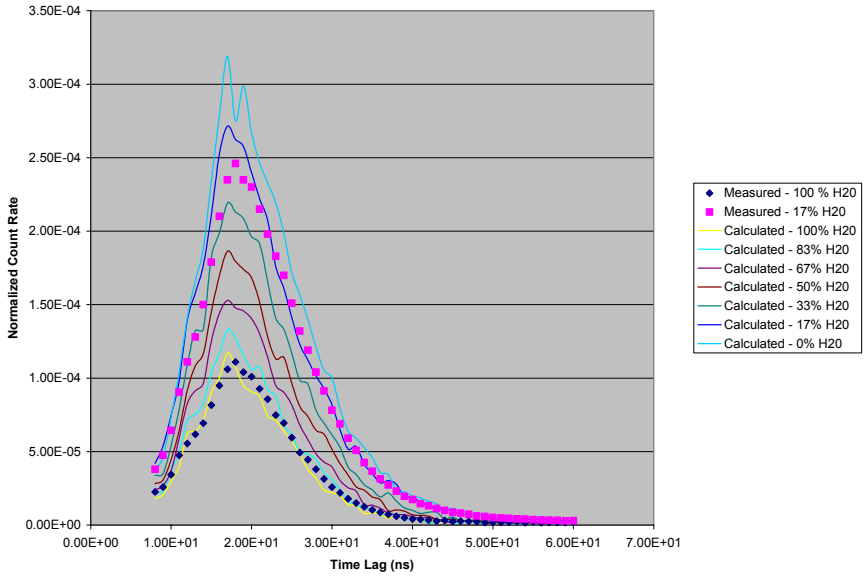

Fig. 2.5.1. Neutron peak transmission simulations and measurements for varying water content for B_4C content of ~4.6 wt%.

[§] The code is a modification of the MCNP 4C code. The cross sections used in these simulations are the ENDF-60C cross sections available in standard MCNP.

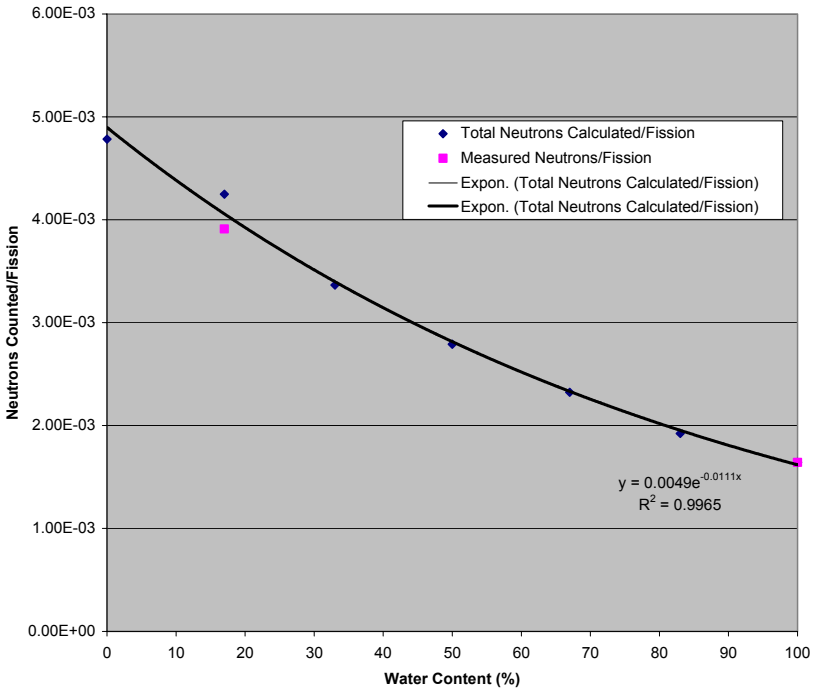

Fig. 2.5.2. Area of neutron peak transmission simulations as a function of water content for 8-in.-thick blocks of 4 wt% B_4C and measurements.

The Monte Carlo calculations provided the functional dependence of the neutron transmission on water content. This functional dependence or sensitivity to water content with the measured data for the nominal BoroBond™ composition can be used to determine the water content of unknown BoroBond™ samples. Although this was done for BoroBond™ blocks, the same procedure can be used for the actual RCSBs once an initial calibration measurement is performed.

To adjust for the calculational bias, the calculated values were adjusted to the experimental value at 100% water content. The resulting functional dependence on water content was fit with an exponential, which can be inverted to give the water content (w) as a function of the neutron counts per Cf fission (n)

$$w = -90.1 \cdot \ln n - 475.8 \qquad (2.5.1)$$

This equation can be used to find the water content independently of the B_4C content of the 8 in. blocks. Table 2.5.1 shows the result of this estimate for all the 8 in.-thick combinations of blocks. The normalized neutron counts (n) were found by integrating the transmission measurements for time lags 6 to 60 ns. The differences may result from the differences in atomic densities for different combinations of blocks since the 2-in.-thick blocks were slightly denser than the 4-in.-thick blocks. The error in the prediction of water content for all unbaked blocks is 8% at worst (D blocks). In the case of the blocks where the water content was reduced by bake-out, the errors are greater. This difference might be explained by considering the error introduced by the bake-out process (see Table B7 in Appendix B).

Table 2.5.1. Predicted water content in 8-in.-thick blocks

Block numbers	Presumed water content (%)	Experimental neutron transmission (*n*)	Predicted water content
A1, A3	100	1.56E-03	106
A2, A4	17	4.00E-03	21.6
B1, B3	100	1.64E-03	102
B2, B4	17	3.91E-03	23.7
C1, C3	100	1.68E-03	100[a]
C2, C4	17	4.11E-03	19.3
D1, D3	100	1.53E-03	108
D2, D4	17	3.81E-03	26.2

[a]Equation used normalized to data for 4.6 wt% B_4C blocks (C blocks) with 100% water so agreement is perfect at that point.

A similar analysis was performed for the 10-in.-thick block combinations. Figure 2.5.3 shows the Monte Carlo simulation performed with the MCNP-PoliMi code and the measured data for the 10-in.-thick combinations of unbaked blocks with 4.6 wt% B_4C. The Monte Carlo calculated integral of the neutron peak as a function of water content is given in Fig. 2.5.4 and compared with the measured.

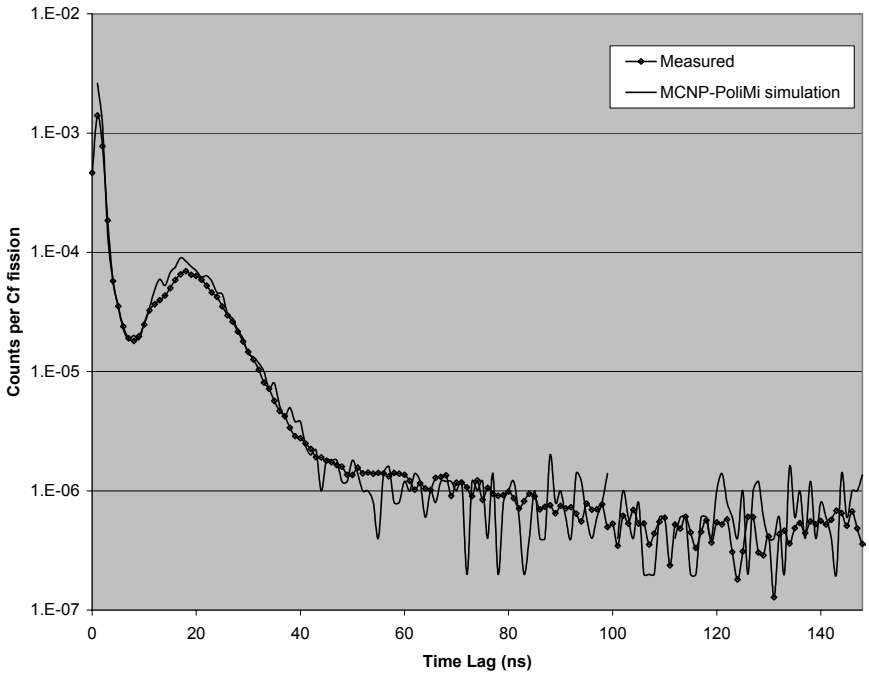

Fig. 2.5.3. Time-of-flight transmission measurement and MCNP-PoliMi simulation for the 10-in.-thick unbaked blocks.

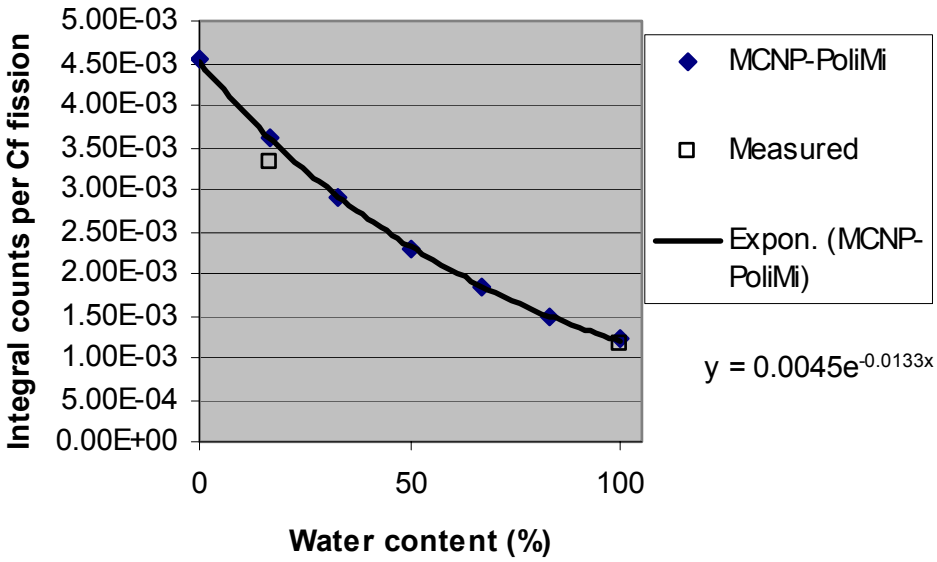

Fig. 2.5.4. Area of neutron peak transmission simulations as a function of water content for 10-in.-thick blocks with ~4.6 wt% B_4C content and measurements.

The Monte Carlo results were fit with an exponential, which can be inverted to give the water content (w) as a function of the normalized neutron counts (n) for the 10 in. blocks

$$w = -75.2 \cdot \ln(n) - 406.16 \tag{2.5.2}$$

This equation can be used to find the water content independently of the B_4C content of the 10 in.-thick combination of blocks. Table 2.5.2 shows the result of this estimate for combinations of blocks with varying B_4C content. The integral neutron counts (n) were found by summing the transmission measurements for time lags 6 to 60 ns. As it can be seen, the proposed equation predicts the full water content with very good approximation: the error is 6% in the worst case for full water content and 9.1 wt % B_4C block and average of ~3%. The reduced water content is overestimated in all cases. Variations in water content are not expected to be as large as produced after baking out the blocks at 140°C.

These two thicknesses of blocks were chosen for this analysis since these thicknesses are close to the distance between fissile storage locations in the RCSB. The total integral counts in the neutron distribution could be measured to a few percent which will yield estimates of the water content of ± 3% for full water content which is the normal composition of the BoroBond™.

Table 2.5.2. Predicted water content in 10-in. thick blocks

Block numbers	Presumed water content (%)	Experimental neutron transmission (*n*)	Predicted water content (%)
A1, A3, A5	100	1.15E-03	103
A2, A4, A6	17	3.41E-03	21.1
B1, B3, B5	100	1.17E-03	101
B2, B4, B6	17	3.32E-03	23.1
C1, C3, C5	100	1.19E-03	100
C2, C4, C6	17	3.46E-03	19.9
D1, D3, D5	100	1.09E-03	106
D2, D4, D6	17	3.20E-03	25.8

3. ^{3}He THERMAL NEUTRON COUNTING

The total neutron count rate and the epithermal neutron count rate in ^{3}He proportional counters was measured for both the blocks and the RCSB. The epithermal neutron count rate was measured by surrounding the counter with 0.045-in.-thick cadmium. These count rates are related to the thermal and epithermal neutrons that are available to induce fission in uranium stored in RCSBs. These measurements were all performed with the BoroBond™ material between the source and the detectors.

3.1 NEUTRON COUNTER DESCRIPTIONS

The ^{3}He proportional counters used in the measurements were Reuter Stokes model number RS-P4-611-101 which had a 10.4-in.-active length, 2-in.-diam., and were filled with ^{3}He to a pressure of 4 atm. The detectors were designed for this application. The detector structural material was 0.055-in.-thick aluminum (1100) tubing. The details of the detector are shown in Fig 3.1.1.

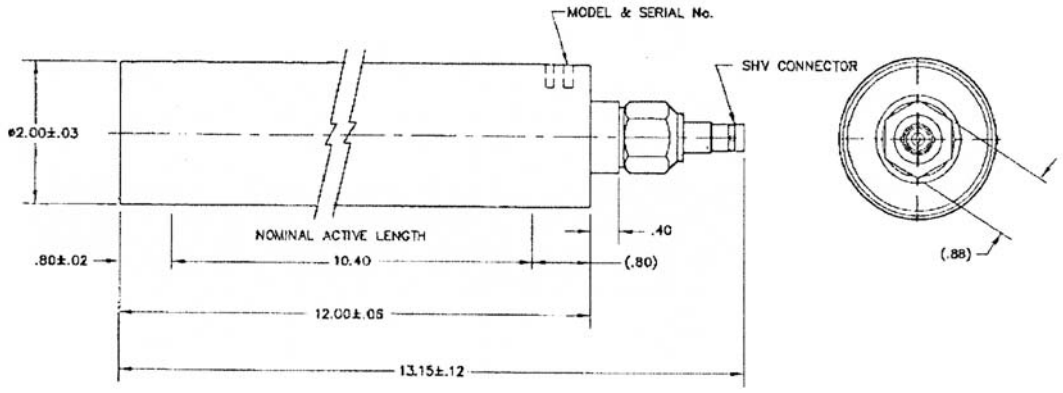

Fig. 3.1.1. Sketch (vendor provided) of the ^{3}He proportional counter for neutron counting measurements.

3.2 BLOCK MEASUREMENTS

The experimental arrangement of the source and detectors for neutron counting for the block measurements is shown in Fig. 3.2.1. To minimize floor reflection effects the blocks were raised so that the bottom of the blocks was 66.5 in. above the floor. The sources were under the blocks. Six small ^{252}Cf pellet sources were located in a 12x12x0.5-in.-thick piece of Styrofoam (density = 0.0264 g/cm^3). Based on relative count rate measurements with ^{3}He detectors (described in Appendix C), the total neutron output of the six pellet sources is 1.94×10^6 neutrons per sec on October 18, 2002. The pellet sources were centered and arranged on the corners and centers of the long sides of a rectangle (3 by 2.5 in.). The long sides of the rectangle were parallel to the centerline of the detectors. Another source in an ionization chamber (Cf44) was located adjacent to the lower surface of the Styrofoam. The neutron intensity of this source on October 18, 2002, from the measurements of Appendix C was 3.94×10^6 n/sec. The Styrofoam was below the blocks and on a 0.125-in.-thick carbon steel platform that was part of the lifting device shown in Fig. 2.3.1. The ^{3}He proportional counters were on top of the blocks enclosed in a 0.062-in.-thick aluminum box that had 0.030-in.-thick cadmium on the outside surface at the top and side. The cadmium of the aluminum box surrounding the detectors absorbed thermal neutrons returning from the walls and ceiling of the room. One of the detectors inside the box (detector 1) was not Cd covered and the other detector was covered with 0.045-in.-thick Cd. Thus, detector 1 detected all slow neutrons and detector 2 those above the Cd cutoff energy. As the thickness of the blocks varied the distance between the sources and detector also changed, so the data is affected by and contains this geometric effect. The active length of the detectors was centered on the blocks, and the centerline of the two detectors was separated by 4.875 in. These measurements were performed in the 60x60x30ft High Bay of the Bldg 3500 at ORNL to minimize room return effects and were located 20 ft. from the nearest wall. The data obtained in these counting measurements are given in Appendix B.

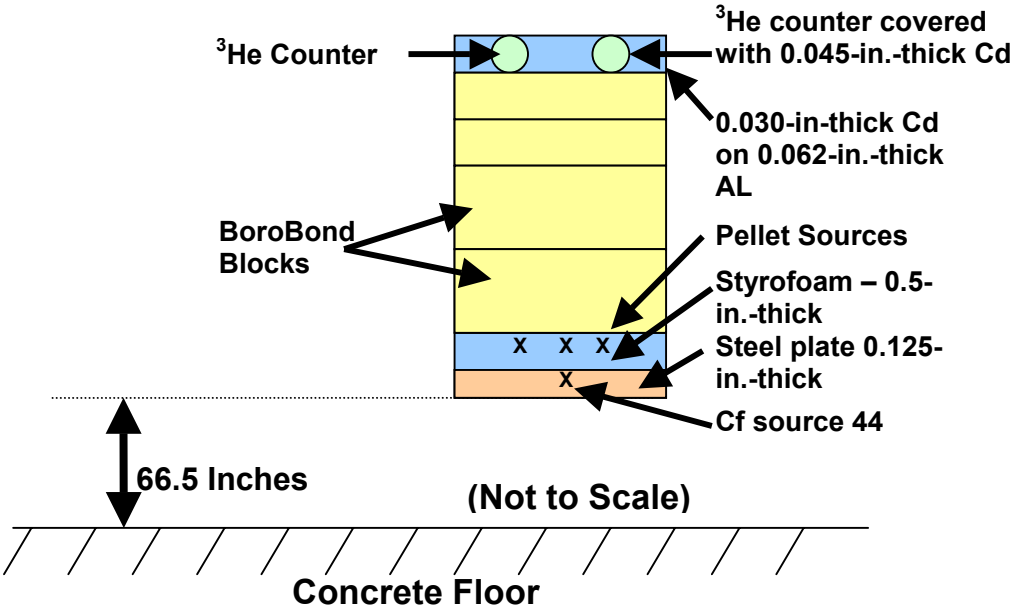

Fig. 3.2.1. Sketch of the source-detector block configuration for the neutron counting measurements.

The average total count rates are plotted as function of block thickness in Fig. 3.2.2 for the unbaked blocks. Except for the blocks with no boron, the count rate decreases with thickness to about 100 cps for the 12-in.-thickness. For the blocks with no B_4C, the count rate increases between 2 and 4 in. almost a factor of two. This results from the fact that the geometric effect is overwhelmed by the effect of the factor of two increases in moderator thickness.

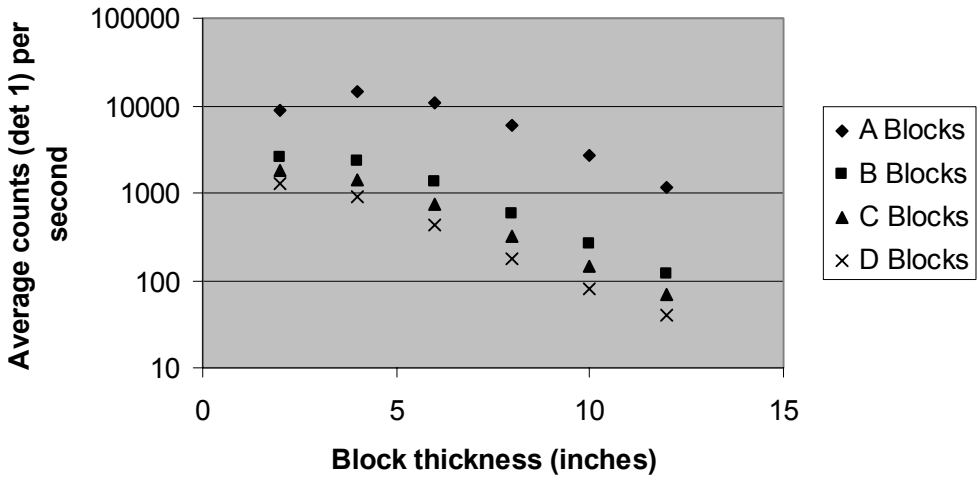

Fig. 3.2.2. Average count rate in detector 1 for unbaked blocks and varying B_4C content as a function of block thickness.

Similar data for the baked blocks are given in Fig 3.2.3. With lower water content, the count rates are reduced by approximately an order of magnitude for the thinner blocks with no B_4C. Reduced water content results in less low energy neutrons, because the primary neutron slowing material (H_2O) is reduced to ~1/6 of the original value for the unbaked blocks. This effect decreases with thickness until it is very small for thicknesses 8 in. and above. There are a variety of competing effects that are different at different thicknesses and B_4C contents and make this data useful for verifying calculations. These competing effects could be separately quantified using Monte Carlo calculation.

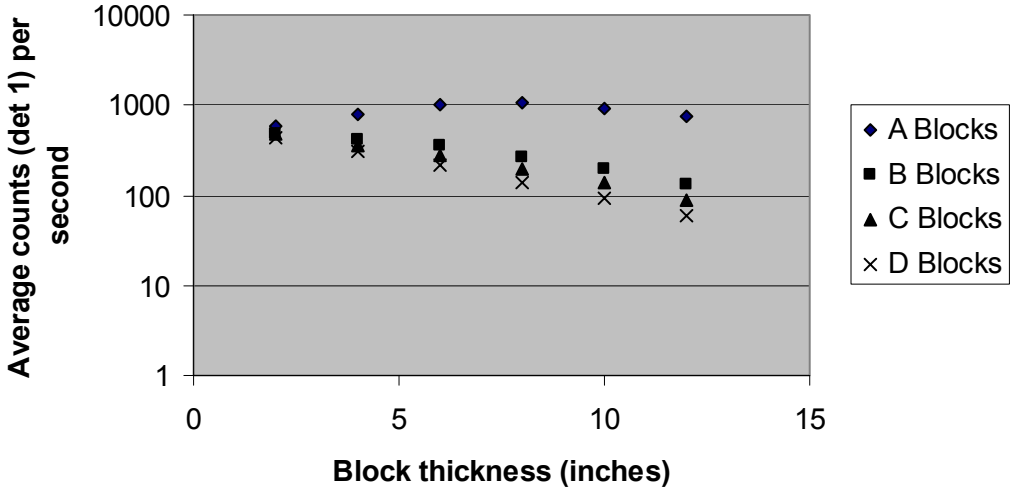

Fig. 3.2.3. Average count rate in detector 1 for baked blocks and varying B_4C content as a function of block thickness.

The thermal neutron count rates were obtained by subtracting the count rates from the detector covered with 0.045-in.-thick cadmium (detector 2) from those for the bare detector (detector 1) 4.875 in. away but symmetrically located with respect to the sources and blocks. The results for the unbaked blocks as a function of block thickness are plotted in Fig. 3.2.4 as a function of block thickness.

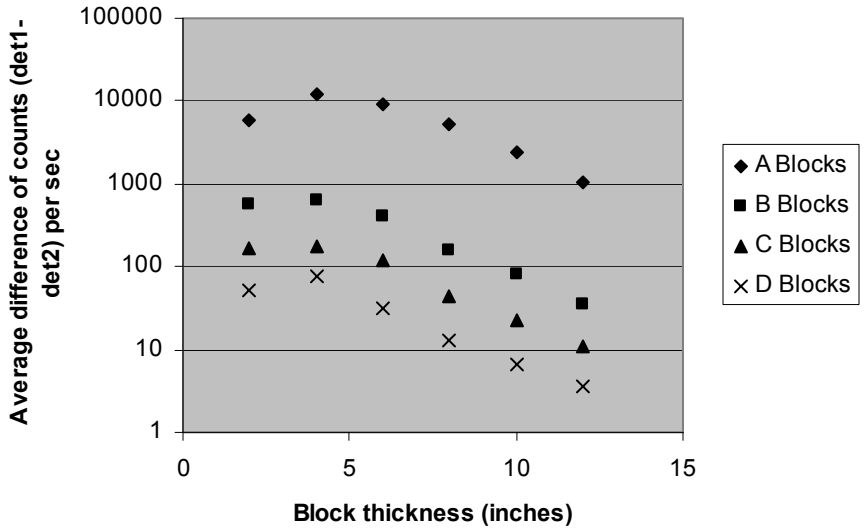

Fig. 3.2.4. Average difference of count rates (det 1 – det 2) for unbaked blocks and varying B_4C content as a function of block thickness.

The thermal neutron count rates are plotted vs. block thickness in Fig. 3.2.5 for the baked blocks. As expected, with the lower water content of the blocks the count rates decrease considerably. For block thickness of 2 to 4 in., the thermal neutron count rate decreases by about an order of magnitude, between the B_4C case (A blocks) and ~9.1 wt% B_4C (D blocks).

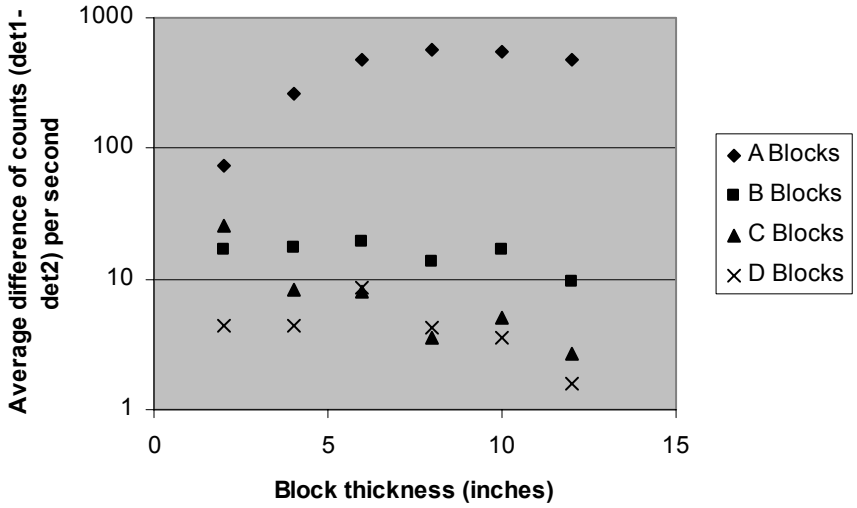

Fig. 3.2.5. Average difference of count rates (det 1 – det 2) for baked blocks and varying B_4C content as a function of block thickness.

The experimental data presented in Fig. 3.2.2 through Fig. 3.2.5 show that the thermal, epithermal, and thermal count rates depend on both the water and B_4C content of the BoroBond™. It follows that these measurements alone cannot be used to obtain both quantities. In Section 4, a method to obtain B_4C content will be outlined for the gamma ray spectrometry data knowing the water content. This could also be done for the neutron counting data. These slow neutron counting measurements measure what neutrons are not captured by boron, whereas gamma ray spectrometry measures what is directly captured by boron.

4. GAMMA RAY SPECTROMETRY

Prompt gamma neutron activation analysis (PGNAA) techniques as well as gamma spectroscopy for gammas produced by the inelastic scattering of neutrons from BoroBond™ constituents were employed in this study. Measurements were performed for the blocks of varying B_4C and water content and for the RCSB. All gamma ray spectrometry measurements have a measured live time in the multichannel analyzer of 1000 sec and used a HPGe gamma ray detector. Goals for this portion of the project included investigation of Monte Carlo models and experimental measurements as methods for deriving wt% B_4C calibration curves for the RCSB.

4.1 PROMPT CAPTURE GAMMA RAYS FROM NEUTRON ACTIVATION

Prompt gamma neutron activation analysis (PGNAA) techniques are widely used for the determination of elemental composition of samples. PGNAA relies on the detection of prompt gamma rays produced subsequent to the capture of thermal neutrons by sample constituents. For this study, the interactions of interest are with the energy of the emitted gamma ray in parenthesis:

$$
\begin{aligned}
&^{23}\mathrm{Na}\ (n,\gamma)\ ^{24}\mathrm{Na}\quad (472.2\ \mathrm{keV})\\
&^{186}\mathrm{W}\ (n,\gamma)\ ^{187}\mathrm{W}\quad (474\ \mathrm{keV})\\
&^{10}\mathrm{B}\ \ (n,\alpha)\ ^{7}\mathrm{Li}^{*}\quad (478\ \mathrm{keV})\\
&^{23}\mathrm{Na}\ (n,\gamma)\ ^{24}\mathrm{Na}\quad (499.4\ \mathrm{keV})\\
&^{39}\mathrm{K}\ \ (n,\gamma)\ \ ^{40}\mathrm{K}\quad\ (770.3\ \mathrm{keV})\\
&^{1}\mathrm{H}\ \ \ (n,\gamma)\ \ ^{2}\mathrm{H}\quad\ \ (2223.3\ \mathrm{keV})\ .
\end{aligned}
$$

Tungsten is of interest since it was the material used to shield the HPGe gamma ray detector from the gamma rays from ^{252}Cf fission. The primary reaction of interest for this study is neutron capture in boron with the subsequent release of a 478 keV gamma ray.

$$
\begin{gathered}
^{10}\mathrm{B} + \mathrm{n} \rightarrow {}^{7}\mathrm{Li}^{*} + \alpha\\
\sigma\\
\sigma_{abs}\ (0.025\mathrm{ev}) = 3837\ \mathrm{b}\\
{}^{7}\mathrm{Li}^{*} \rightarrow {}^{7}\mathrm{Li} + \gamma\ (478\ \mathrm{keV})
\end{gathered}
$$

The 478 keV gamma ray, produced by the recoiling excited lithium nucleus from neutrons captured in ^{10}B, is easily recognized in gamma spectra due to the Doppler-broadening of the gamma line by 11-15 keV. Figure 4.1.1 presents a portion of the spectrum from a typical measurement and illustrates this broadening. Also shown on this figure is the 511 keV gamma ray from the positron-electron annihilation reaction which is not Doppler broadened.

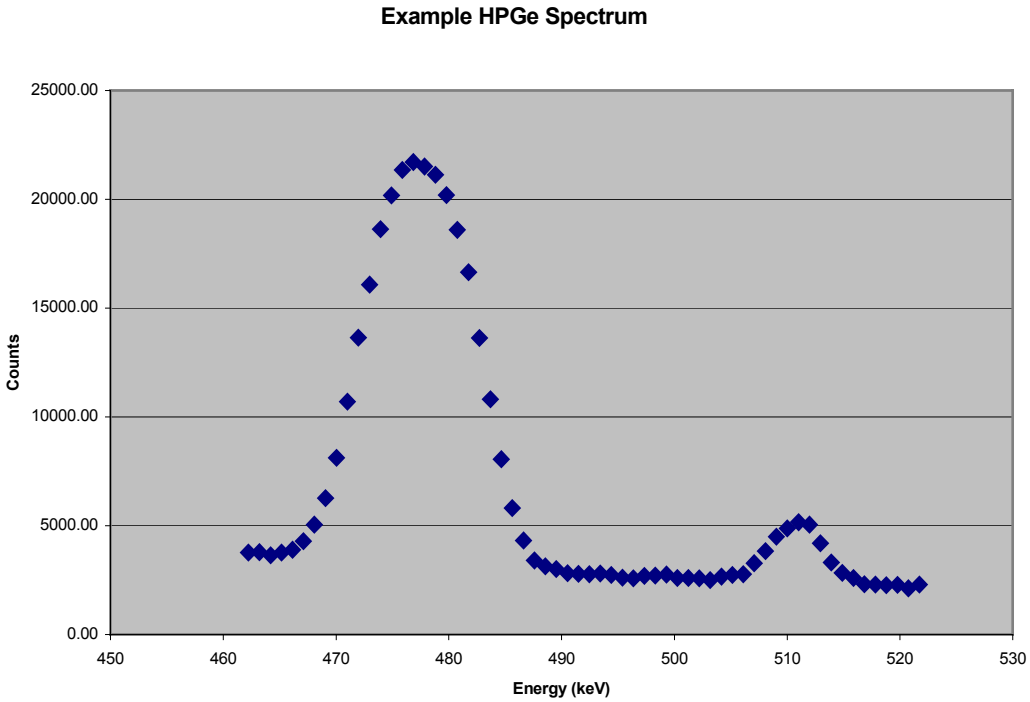

Fig. 4.1.1. Portion of a typical gamma spectrum illustrating Doppler-broadened boron peak at 478 keV.

4.2 BLOCK MEASUREMENTS

Gamma spectroscopy measurements were performed with a variety of exploratory configurations of source and detector and tungsten alloy shield. However, a single experimental arrangement was found that could be used for both the sample blocks and the test RCSB. Figure 4.2.1 presents the arrangement of (6) stacked ^{252}Cf pellet sources centered on the tungsten shield (a 4x4x4 in. tungsten alloy block) and a high-purity germanium (HPGe) detector against a 12×12-in. BoroBond block. This arrangement located the source and the centerline of the detector the same distance from the middle of the BoroBond™ block and at the vertical centerline. The tungsten block provided a high-density shield for lowering ^{252}Cf source gamma flux at the HPGe detector. Most of the measurements were performed with the arrangements of Fig. 4.2.1A and 4.2.1B. This arrangement was chosen so that the block measurements and the RCSB measurements would have a common geometry, i.e. source-shield-detector against a flat surface.

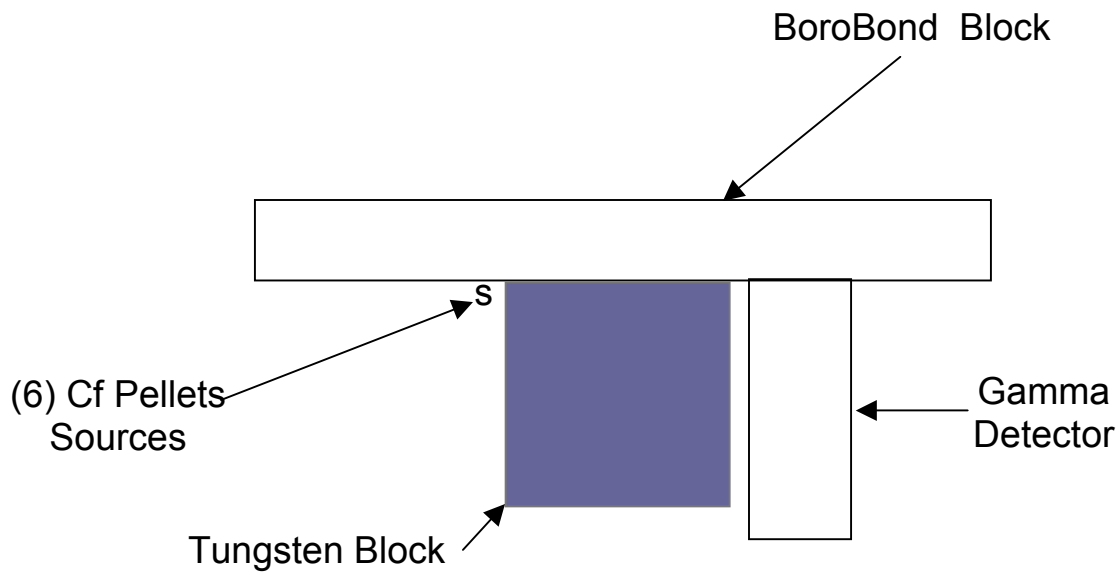

Fig. 4.2.1A. Gamma spectroscopy experimental arrangement (top view).

The ^{252}Cf pellet sources had a combined source strength of 1.94×10^6 neutrons per second as of October 18, 2002. The tungsten alloy block was composed of 95% tungsten, 4% nickel, and 1% copper. The tungsten was alloyed in order to allow easier machining of the block. The HPGe detector was an ORTEC coaxial, p-type detector and was the only one available at the time of these measurements. Future research efforts should consider the use of n-type HPGe detectors due to reduced dead layer thickness (better detection efficiency at low energies) and reduced neutron damage effects (better energy resolution).

Signal-processing electronics included the built-in preamplifier for the HPGe detector, an ORTEC 671 spectroscopy amplifier, and an ORTEC Trump-8k multichannel analyzer buffer with associated ORTEC Maestro analysis software.

Fig. 4.2.1B. Gamma spectroscopy experimental arrangement (side view).

4.2.1 Boron Capture Gamma Ray Measurements

The sample blocks were measured for various thicknesses using various combinations of the 2 and 4 in. blocks for a given B_4C concentration. These combinations are presented in Table 4.2.1. The wt% B_4C of the series A, B, C, and D blocks was 0, 2.3, 4.6, and 9.1, respectively.

Variance-weighted average values for integral counts in the boron peak are presented in Figure 4.2.2. Values for individual measurements are provided in Table D4. Variance-weighted average values are provided in Table D5. Average values presented in Figure 4.2.2 and hereafter are not corrected for ^{23}Na and ^{186}W thermal neutron capture interference lines since Monte Carlo calculations and measurements indicated negligible counts due to these two sources. Counts in the boron peak were summed from 465 keV to 490 keV. Note the asymptotic behavior of counts for all B_4C contents at approximately a 6-in. thickness. This asymptotic behavior is a result of few source neutrons penetrating deep into the block, and gamma rays produced not getting back to the detector. This measurement obtains verification for the 6 in. of BoroBond™ adjacent to the source-shielded detector arrangement.[**]

[**] Perhaps the AmBe source proposed at the factory verification which produces ~4 MeV neutron will characterize the material to a slightly greater depth.

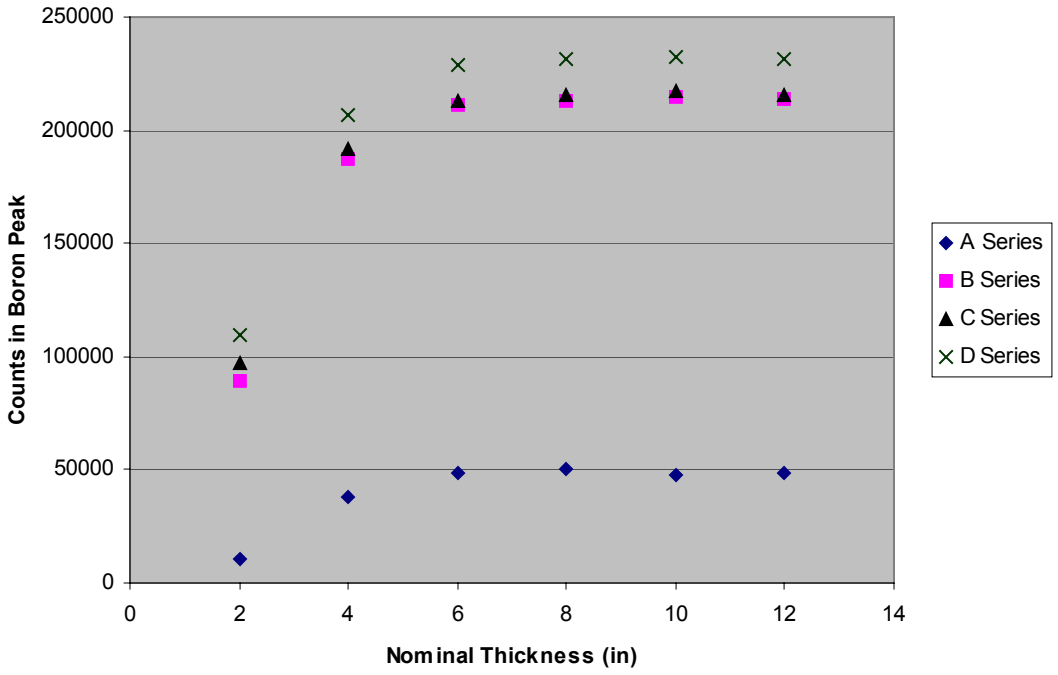

Fig. 4.2.2. Variance-weighted average values for counts in boron peak as a function of unbaked block thickness.

Table 4.2.1. Block combinations measured by gamma ray spectrometry

Block ID[a]	Nominal thickness (in.)
5	2
6	2
7	2
8	2
1	4
2	4
3	4
4	4
5,7	4
6,8	4
1,5	6
2,6	6
1,3	8
2,4	8
1,3,5	10
2,4,6	10
1,3,5,7	12
2,4,6,8	12

[a]The first numbered block was adjacent to the source and the last was farthest from the sources.

While the A-series blocks were nominally 0 wt% B_4C, measurements indicated some trace level of boron was in the blocks. The clearly Doppler-broadened shape of the peaks indicated the presence of boron. Investigations of interfering lines

- ^{23}Na (n,γ) ^{24}Na (472.2 keV)
- ^{186}W (n,γ) ^{187}W (474 keV)
- ^{187}W decay (480 keV)

were conducted. Measurements to quantify the presence of lines from the tungsten block from measurements without the BoroBond™, but with polyethylene, indicated that the tungsten lines contributed in an insignificant way. Measurements with Na samples also indicated no significant contribution to the energy range of the boron peak. Baked A-series block measurements did not indicate the presence of B_4C due to the loss of water (and associated moderation) during bakeout.

Monte Carlo simulations of boron neutron capture as a function of wt% B_4C and block thickness were performed in order to quantify the sensitivity of boron capture counts to wt% B_4C and to verify the asymptotic behavior of counts as a function of block thickness. Figure 4.2.3 presents boron capture counts as function of wt% B_4C for unbaked blocks. Figure 4.2.4 presents boron capture counts as a function of block thickness for unbaked blocks.

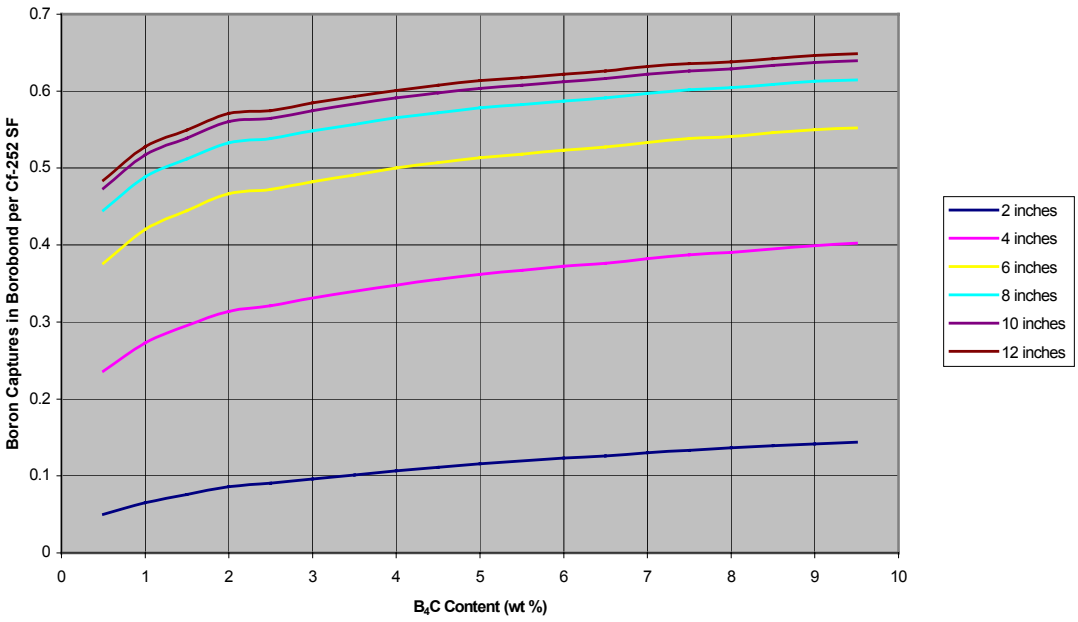

Figure 4.2.3. Monte Carlo simulation of boron captures in blocks per Cf-252 spontaneous fission as a function of wt% B_4C.

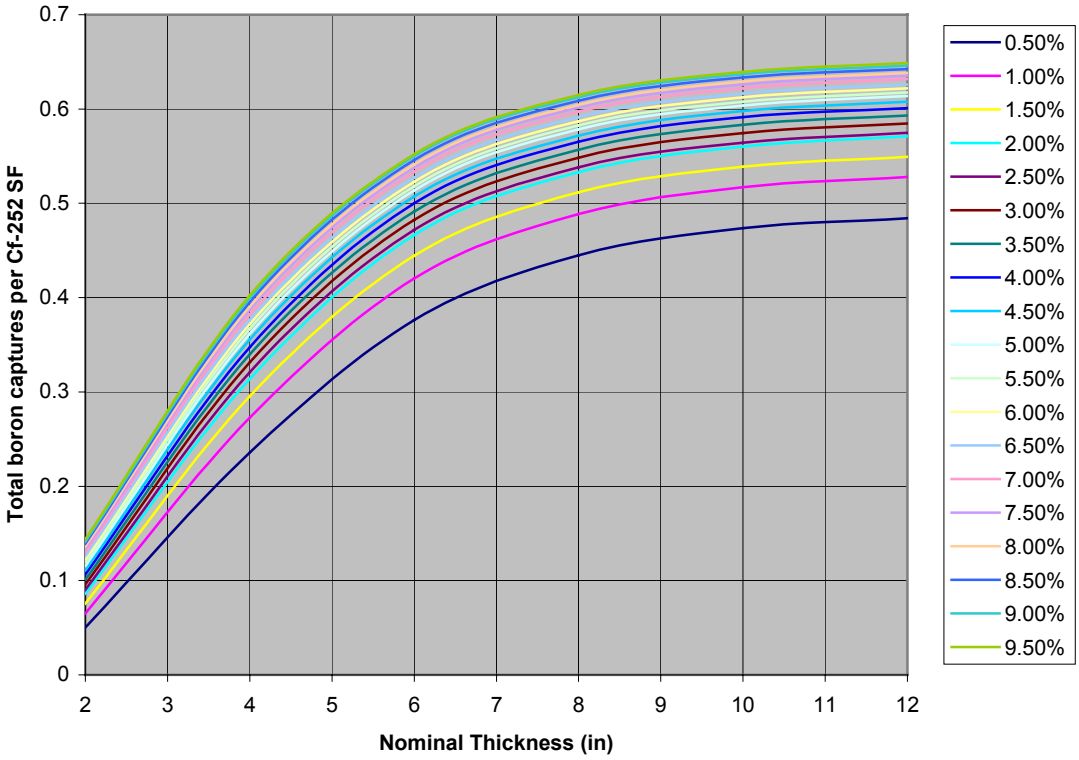

Figure 4.2.4. Monte Carlo simulation of boron captures in blocks per Cf-252 spontaneous fission as a function of nominal block thickness.

Monte Carlo simulations verified the asymptotic behavior of boron peak counts as a function of block thickness. These simulations, however, only modeled neutron captures in the blocks and not the subsequent transport and detection of gammas in the HPGe detector. Note that the asymptote for the simulations is reached at approximately the 9-in. thickness of blocks, as compared to the measured value of approximately 6 in. Because of these differences in modeled and measured values of "boron detections", it was decided that wt% B_4C calibration curves for the RCSB could be best derived from the experimental measurements of the blocks.

In order to determine the sensitivity of the measurement method to B_4C content for a given material thickness, previous data are plotted in Figure 4.2.5 as counts in the boron peak versus nominal B_4C content. Note the relative insensitivity to B_4C content as indicated by the slope of the curves above 2% B_4C. The measured values at 4.6 wt% of B_4C look slightly low when compared to those at 2.3 and 9.1 wt % B_4C.

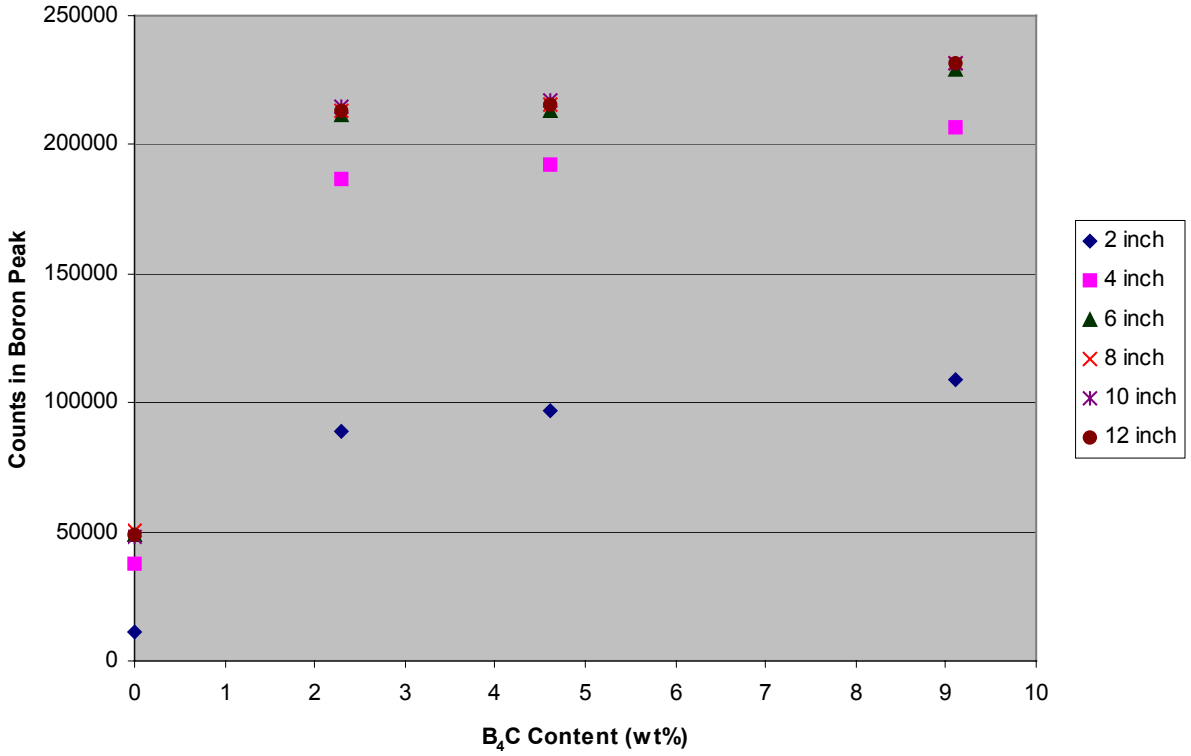

Fig. 4.2.5. Variance-weighted average values for counts in the boron peak as a function of the nominal boron concentration (unbaked).

We first assumed that the slopes for the data series in Figure 4.2.5 were linear over the range of 2.3 to 9.1 wt% B_4C. Using the variance-weighted average values and the variances for those average values given in Table D5 we estimated the sensitivity and associated error for each block thickness with calculated values given in Table 4.2.2 using the Bayesian Inference Using Gibbs Sampling (BUGS) program. [††]

Table 4.2.2. Sensitivity (wt% B_4C per count in boron peak) and associated error for each block thickness

Nominal Thickness (in.)	Sensitivity (wt% B_4C/count)	1-σ Sensitivity error (wt% B_4C/count)
2	3.42e-4	1.53e-4
4	3.43e-4	3.10e-4
6	3.53e-4	6.12e-4
8	3.33e-4	6.12e-4
10	3.65e-4	6.12e-4
12	3.49e-4	6.12e-4

[††] WinBUGS 1.4, MRC Biostatistics Unit, Cambridge UK, 2003

The BUGS program was also used to estimate the uncertainty in wt% B_4C given counts in the boron peak by accounting for uncertainties in all of the linear model fitting parameters as well as errors in the measurements. Uncertainties for each block thickness are presented in Table 4.2.3.

Table 4.2.3. Estimated wt% B_4C uncertainty for each block thickness

Nominal Thickness (in.)	B_4C Uncertainty (wt% B_4C)
2	0.10
4	0.32
6	1.08
8	1.01
10	0.93
12	0.95

We concluded that B_4C content may be estimated to ±1 wt% B_4C for blocks of similar composition and geometry.

After baking half (even-numbered blocks) of the blocks to 140°C, measurements were repeated for all block combinations. It was estimated that baking to 140°C would release 5/6 of the water in the BoroBond™ blocks. The baked A-series blocks (0 wt% B_4C) showed no boron peak due to reduced neutron thermalization as a result of the removal of water by baking and only trace amounts of boron. Figure 4.2.6 presents variance-weighted average values of counts in the boron peak for the measurements with blocks after baking. Again, note the asymptotic behavior at approximately 8 in. of material for all B_4C.

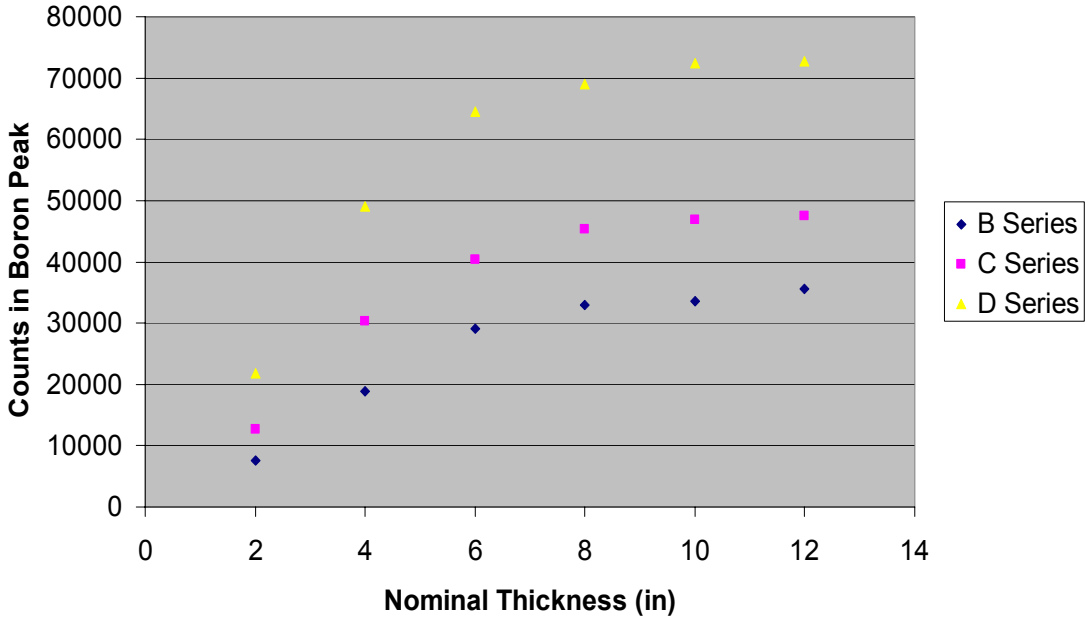

Fig. 4.2.6. Variance-weighted average values for counts in the boron peak as a function of the baked block thickness.

Figure 4.2.7 presents combined results for unbaked and baked measurements. As expected, the loss of hydrogen results in a significant reduction of the counts in the boron peak due to reduced thermalization of neutrons.

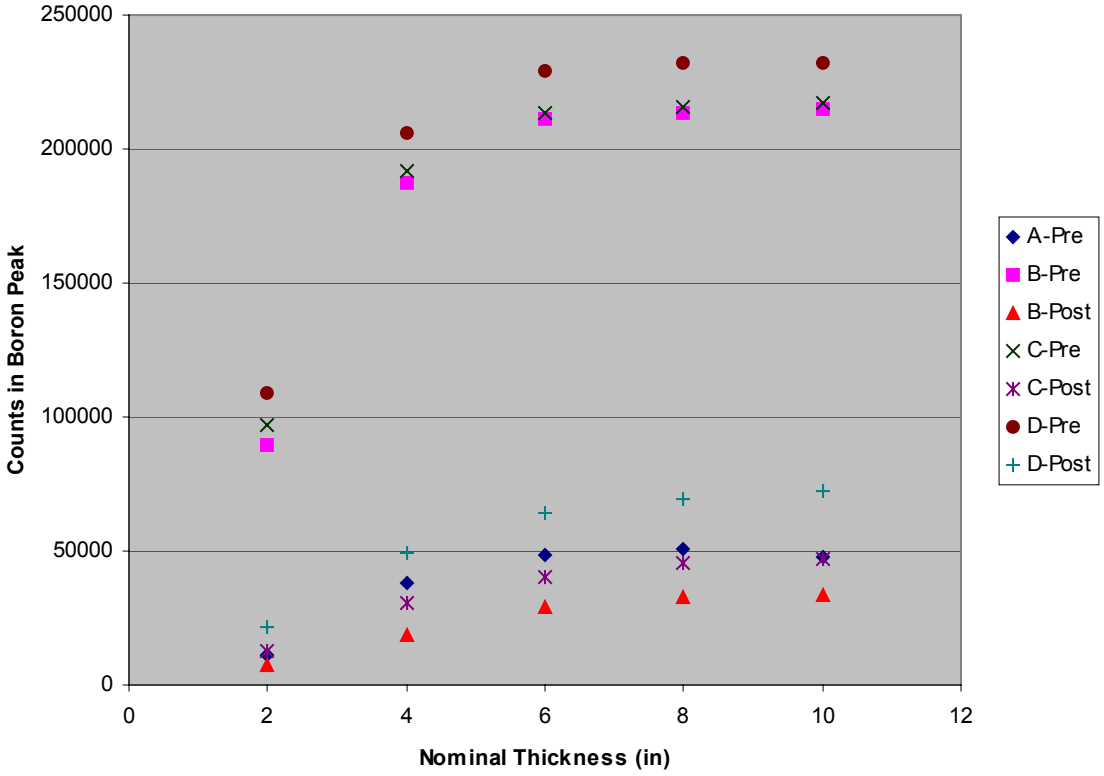

Fig. 4.2.7. Variance-weighted average values for counts in the boron peak as a function of the block thickness for the unbaked and baked blocks.

In the same manner as for the prebake measurements, we determined the sensitivity of the measurement method to B_4C content for a given material thickness. Post-bake data are plotted in Figure 4.2.8 as counts in the boron peak versus nominal B_4C content. Table 4.2.4 presents estimated sensitivity and associated error for each block thickness.

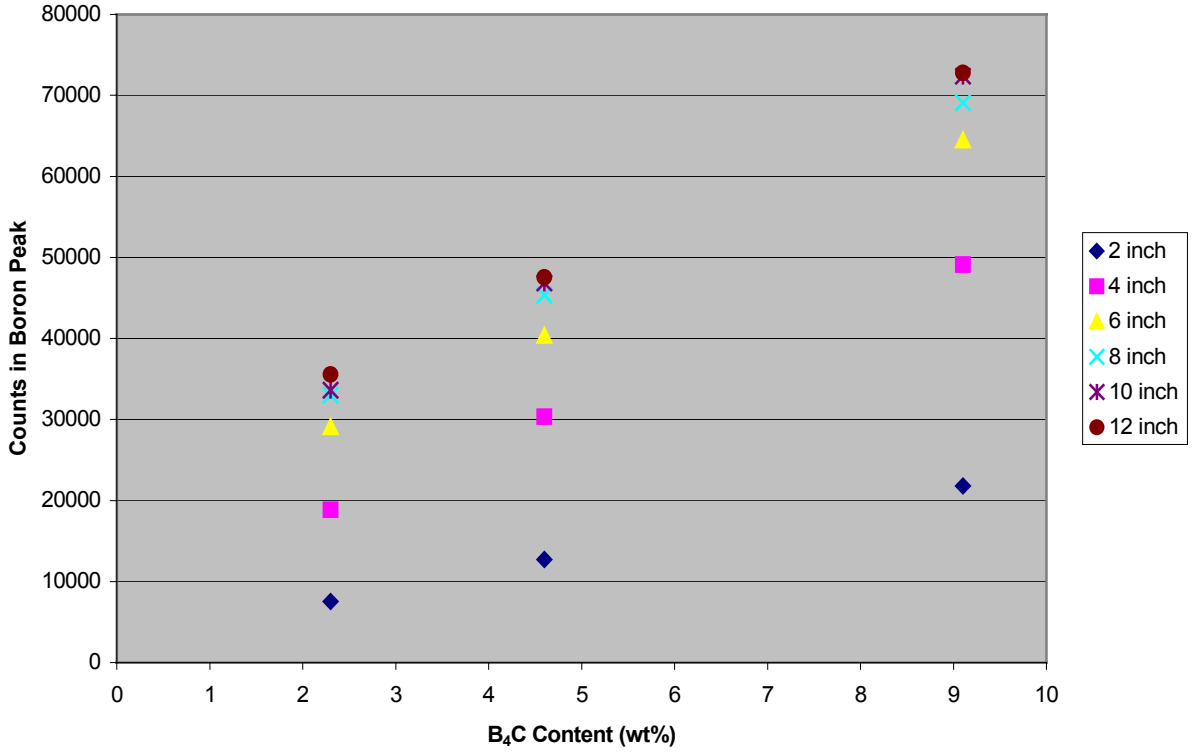

Fig. 4.2.8. Variance-weighted average values for counts in the boron peak as a function of the nominal boron concentration for the baked blocks.

Table 4.2.4. Sensitivity (wt% B_4C per count in boron peak) and associated error for each block thickness (baked blocks)

Nominal Thickness (in.)	Sensitivity (wt% B_4C/count)	1-σ Sensitivity error (wt% B_4C/count)
2	4.80e-4	1.53e-4
4	2.26e-4	2.33e-4
6	1.92e-4	5.10e-5
8	1.89e-4	4.03e-5
10	1.76e-4	3.57e-5
12	1.82e-4	4.59e-5

The BUGS program was also used to estimate the uncertainty in wt% B_4C given counts in the boron peak. Uncertainties for each block thickness are presented in Table 4.2.5.

Table 4.2.5. Estimated wt% B_4C uncertainty for each block thickness (baked blocks)

Nominal Thickness (in.)	B_4C Uncertainty (wt% B_4C)
2	.07
4	.16
6	.07
8	.06
10	.06
12	.07

Note the order of magnitude decrease in B_4C wt% uncertainty after baking the blocks while the sensitivity (Tables 4.2.2 and 4.2.4) does not differ significantly. The lower uncertainty for baked blocks is probably due to the baked data more closely conforming to a linear model than did the unbaked data.

It should be noted that these measurements were complicated due to non-uniform densities among blocks and changing weight concentrations as a function of time (Tables B5 through B7). Calculations in this section did not account for these differences, and thus, assumed nominal values for all blocks.

4.2.2 Hydrogen Capture Measurements

The hydrogen thermal neutron capture line was examined for both unbaked and baked block samples. The Maestro gamma ray spectrometry analysis software consistently recognized the hydrogen peak for unbaked blocks with 0 and 2.3 wt% B_4C composition (A- and B-series blocks). Otherwise, the software did not recognize the hydrogen peak. Fig. 4.2.9 presents average values for A-and B-series blocks measurements.

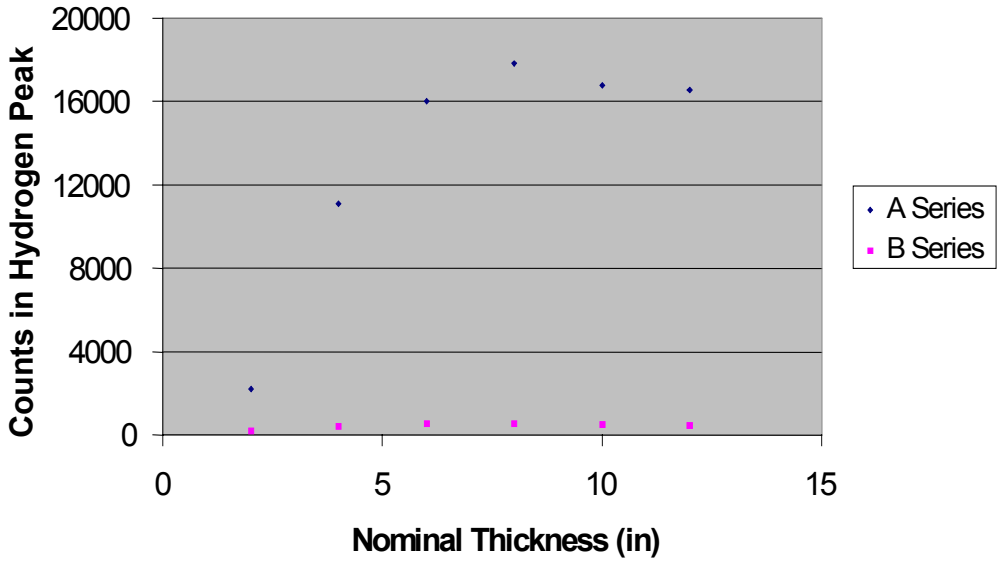

Fig. 4.2.9. Counts in hydrogen peak versus nominal thickness.

As boron concentration increases, hydrogen thermal neutron capture (capture cross section of 0.33 barns) becomes insignificant compared to boron thermal neutron capture (capture cross section of 3837 barns). Based on these measurements, gamma spectrometry measurements would not be useful for the determination of hydrogen content in RCSBs with nominal boron concentration of 4.6 percent.

4.2.3 Inelastic Scattering Measurements

Several inelastic neutron scattering gamma lines of interest were identified prior to the measurement series:

^{31}P (n,n′) ^{31}P (1266.1 keV)
^{24}Mg (n,n′) ^{24}Mg (1368.8 keV)
^{28}Si (n,n′) ^{28}Si (1779 keV)

Values for integral counts in these peaks may prove useful for future modeling efforts, but the measurements indicate widely varying values among blocks of similar nominal composition and thickness. The variance may be due to actual composition differences among blocks. Without additional study, inelastic scattering gammas do not appear to be useful for determination of block and RCSB composition.

4.3 RCSB MEASUREMENTS

Measurements were made using the source detector arrangement of Figure 4.2.1 at points on the mockup RCSB as specified in Figure 4.3.1. The mockup RCSB was filled with 4.6 wt% B_4C BoroBond™. Earlier measurement setups attempted to place the sources and tungsten shielding block in the fissile storage locations while measuring with the HPGe detector on the outside of the mockup RCSB. That arrangement proved clumsy and unrepresentative of the block calibration measurements. Table 4.3.1 presents measurement points grouped by approximate BoroBond™ thickness at the measurement point. Fig. 4.3.2 presents results for boron peak counts at all 13 measurement points.

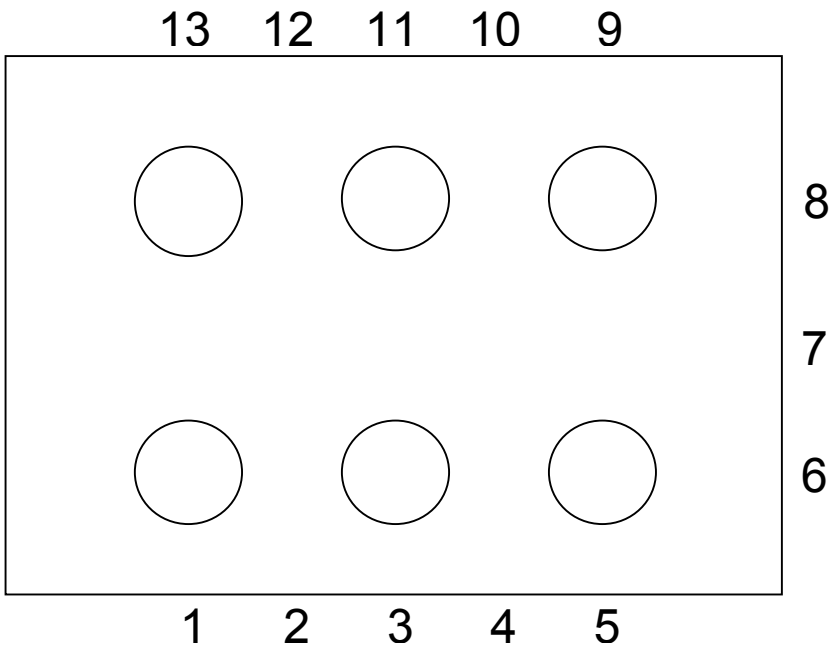

Fig. 4.3.1. RCSB measurement identification numbers.
(Top view, numbers indicate position of the gamma ray spectrometry measurement.)

Table 4.3.1. Measurement points grouped by approximate BoroBond™ thickness

4.3 in. thick BoroBond™	5.5 in. thick BoroBond™	6 in. thick BoroBond™
6,8	1,5,9,13	2,4,7,10,12

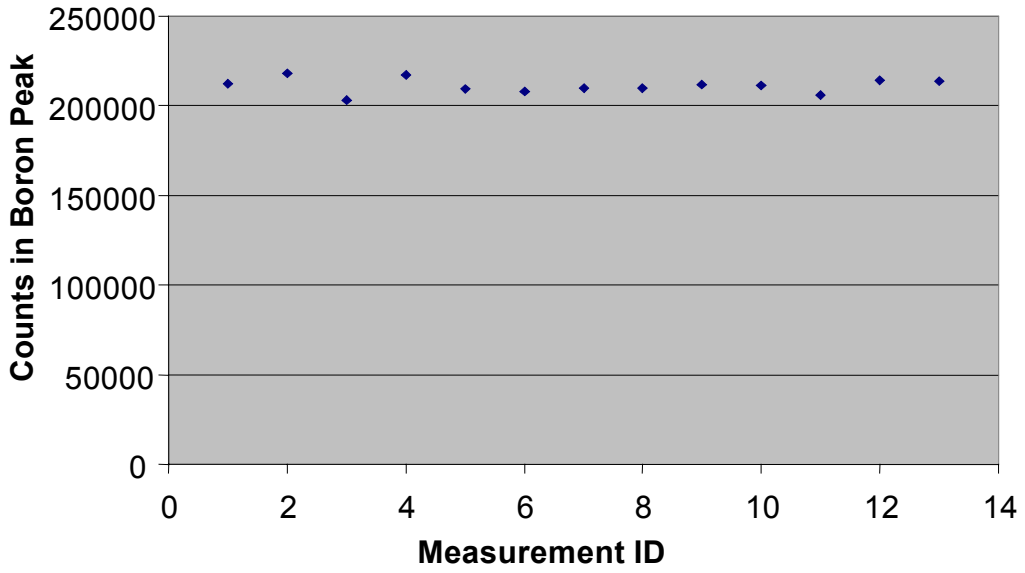

Fig. 4.3.2. Mockup RCSB measurements on the sides using HPGe detector.

Variance-weighted average values of counts in the boron peak for the three groups from Table 4.3.1 are plotted in Figure 4.3.3 as a function of nominal BoroBond™ thickness.

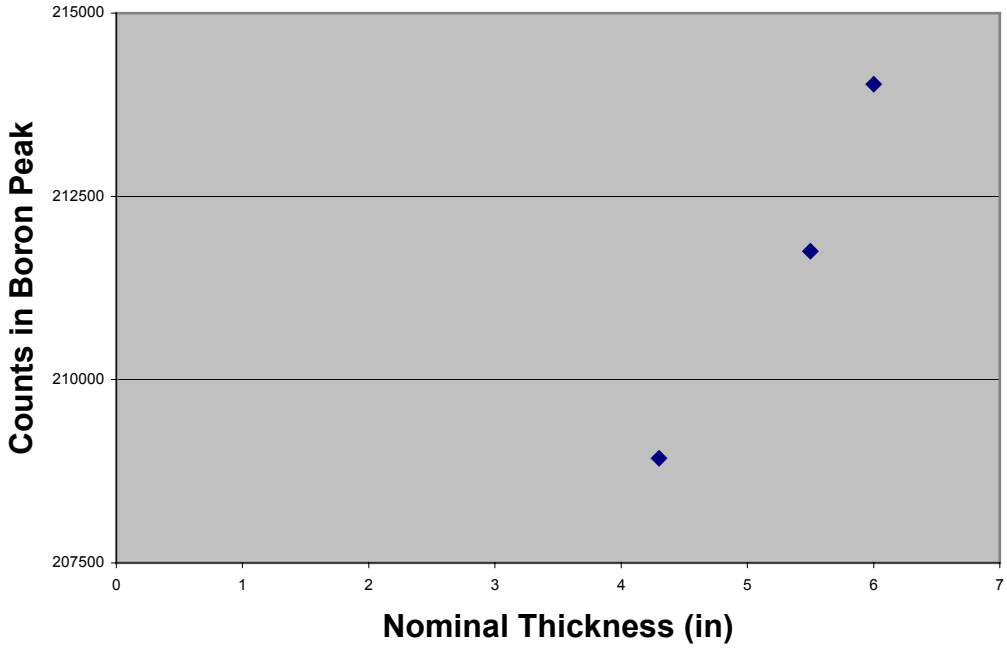

Fig. 4.3.3. Variance-weighted average values of boron peak counts as a function of nominal BoroBond™ thickness.

Using the BUGS program, the predicted wt% B_4C for the ~6-in. thick RCSB measurements was calculated using the variance-weighted average value of boron counts

from Figure 4.3.3 and the linear calibration model from section 4.2. The BUGS program calculation accounts for uncertainty in all linear model parameters as well as errors in the measurements. For the 6-in. RCSB measurements, BUGS predicted 4±1 wt% B_4C.

Using ^{252}Cf as a source requires temporal corrections for the decay of ^{252}Cf. The corrections could be avoided by the use of an AmBe neutron source for gamma spectrometry. An AmBe source is recommended for the at-the-factory verifications of the boron content. There is no significant decay of this source during its use at the factory or in the HEUMF because its half life is 433 years.

4.4 MONTE CARLO SIMULATIONS AND ANALYSIS

To quantify the dependence of gamma ray spectrometry on B_4C content for the RCSB and water content, Monte Carlo calculations are required since it is not practical to obtain RCSBs with varying B_4C and water contents. These calculations will obtain the sensitivity of gamma ray spectrometry results to both water and B_4C content. Measurements with RCSBs with the nominal B_4C and water content will establish the calculational bias. The sensitivity curves adjusted for bias can then be used to obtain the B_4C content if the water content is known from the time-of-flight transmission measurements. This process obtains functional forms for the dependence of the integral counts in the boron peak on water and B_4C content which can then be converted and used to obtain B_4C content if water content is known. These final calculations for the RCSB will include the detector explicitly in the calculational model. This process is illustrated for the blocks in subsequent discussions and is very similar to what will be done for the RCSB. However, the calculations presented here are only boron capture events without the detector response but illustrates the procedure and dependence on water and B_4C content.

Gamma spectrometry measurements to determine the amount of B_4C present in the blocks are based on the detection of the 478 keV gamma ray emitted by the decay of the Li nucleus following the $^{10}B(n,\alpha)$ reaction. The number of these capture reactions was tallied for a number of Monte Carlo simulations performed with the MCNP-PoliMi code. The code output was then analyzed in post-processing step. The simulations were performed for 8-in. blocks and various water and B_4C content.

The result of the simulations for blocks is given in Fig. 4.4.1. As expected, the number of boron captures is a function of both water and B_4C content. Qualitatively, it can be seen that the number of captures is very sensitive to the water concentration inside the block, and not as sensitive to the boron concentration. The sensitivity is greater for the blocks with lower water content for the nominal boron content (~ 4 wt%).

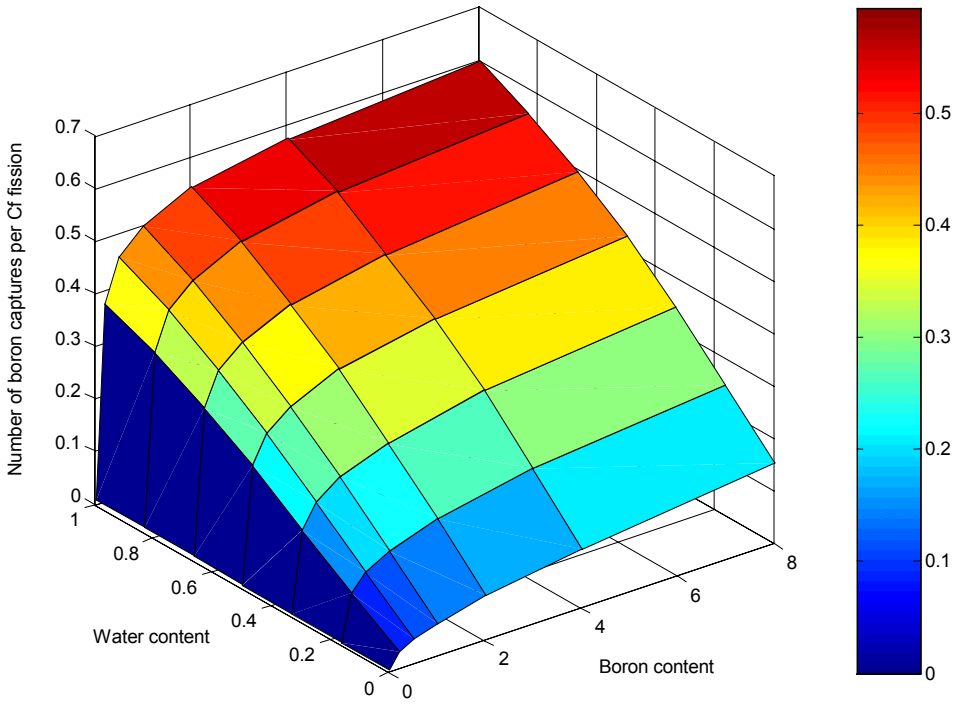

Fig. 4.4.1. Calculated number of boron captures as a function of the B_4C content and the amount of water (wt%).

The results of Fig. 4.4.1 can be plotted as a function of B_4C content for various water contents, as shown in Fig. 4.4.2.

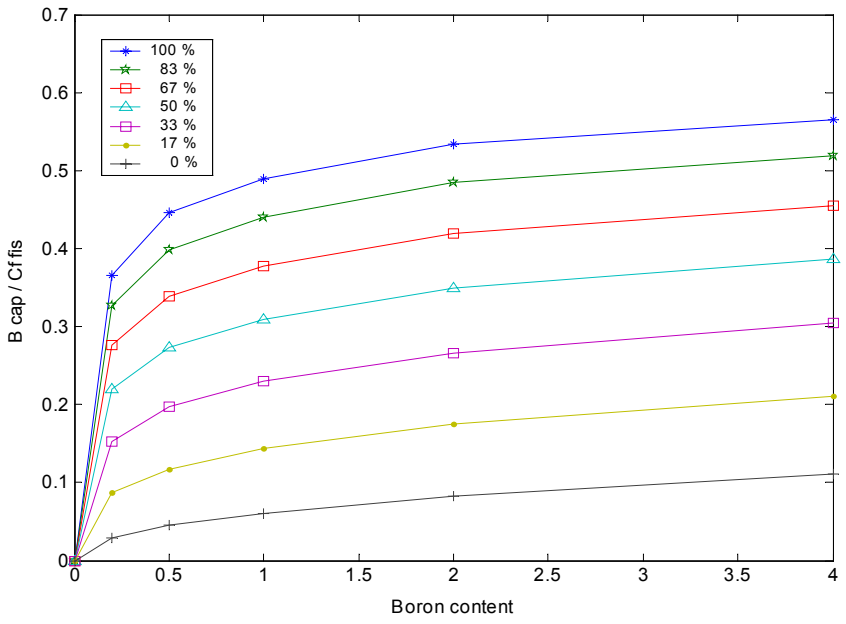

Fig. 4.4.2. Calculated number of boron captures as a function of B_4C content for different amounts of water (wt%).

A fitting procedure was implemented to determine the B_4C content of the sample given the number of boron captures. The functional form was chosen to be of the type

$$n_b = a_1 \cdot b^{0.5} + a_2 \cdot b^{0.25} + a_3 \cdot b^{0.1}, \tag{4.4.1}$$

where n_b is the number of boron captures per ^{252}Cf fission, and b is the B_4C content.

The coefficients a_1, a_2, and a_3 were determined by performing a least squares fit. Table 4.4.1 reports the values of these coefficients for the cases shown are plotted in Fig. 4.4.3 as a function of water content.

Table 4.4.1. Coefficients for Eq. 4.4.1

Water content (%)	a_1	a_2	a_3
100	-0.2762	0.8853	-0.1178
83	-0.2192	0.7413	-0.0802
67	-0.1797	0.6453	-0.0864
50	-0.1378	0.5480	-0.0992
33	-0.0818	0.4103	-0.0979
17	-0.0193	0.2344	-0.0714
0	0.0351	0.0431	-0.0174

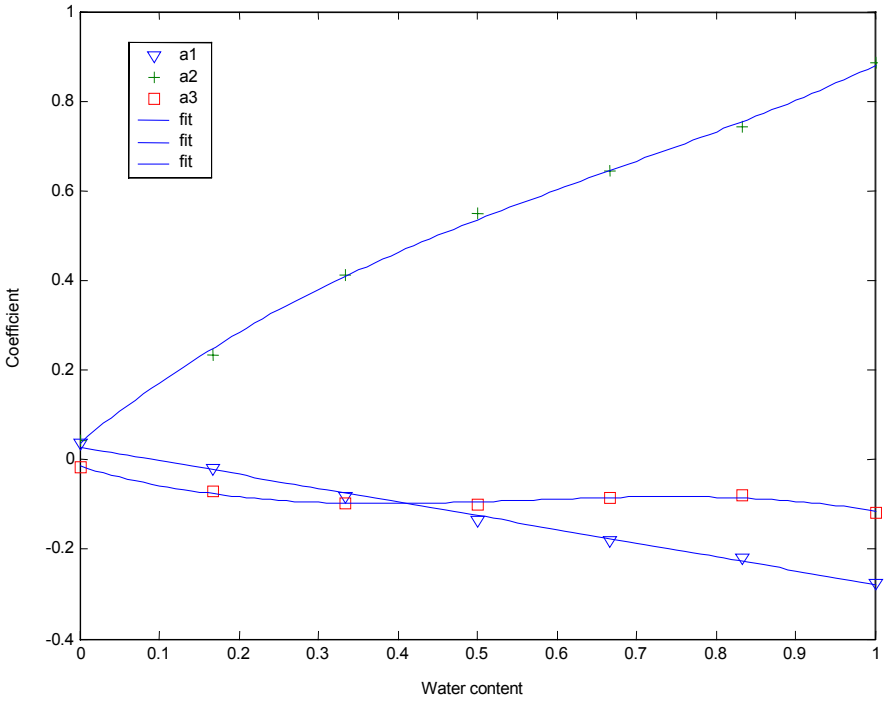

Fig. 4.4.3. Coefficients given in Table 4.4.1 as a function of water content. Also shown are fits to coefficient values.

To determine the amount of boron present in the blocks, it is necessary to first determine how much water is present from the fast neutron transmission measurements. Then, it is possible to determine the coefficients of equation (4.4.1) by using the following fits

$$a_1 = -0.30677w + 0.02783,$$
$$a_2 = 0.6018w^3 - 1.2099w^2 + 1.4505w + 0.03721, \text{ and}$$
$$a_3 = -0.6186w^3 + 1.0452w^2 - 0.5268w - 0.015071. \qquad (4.4.2)$$

where w us the fraction of the total water present.

The fits are shown in Fig. 4.4.4 as a function of B_4C content for various water contents of the blocks. By combining equations 4.4.1 and 4.4.2, it is possible to determine the amount of boron present in the blocks as a function of the amount of water and the number of boron captures.

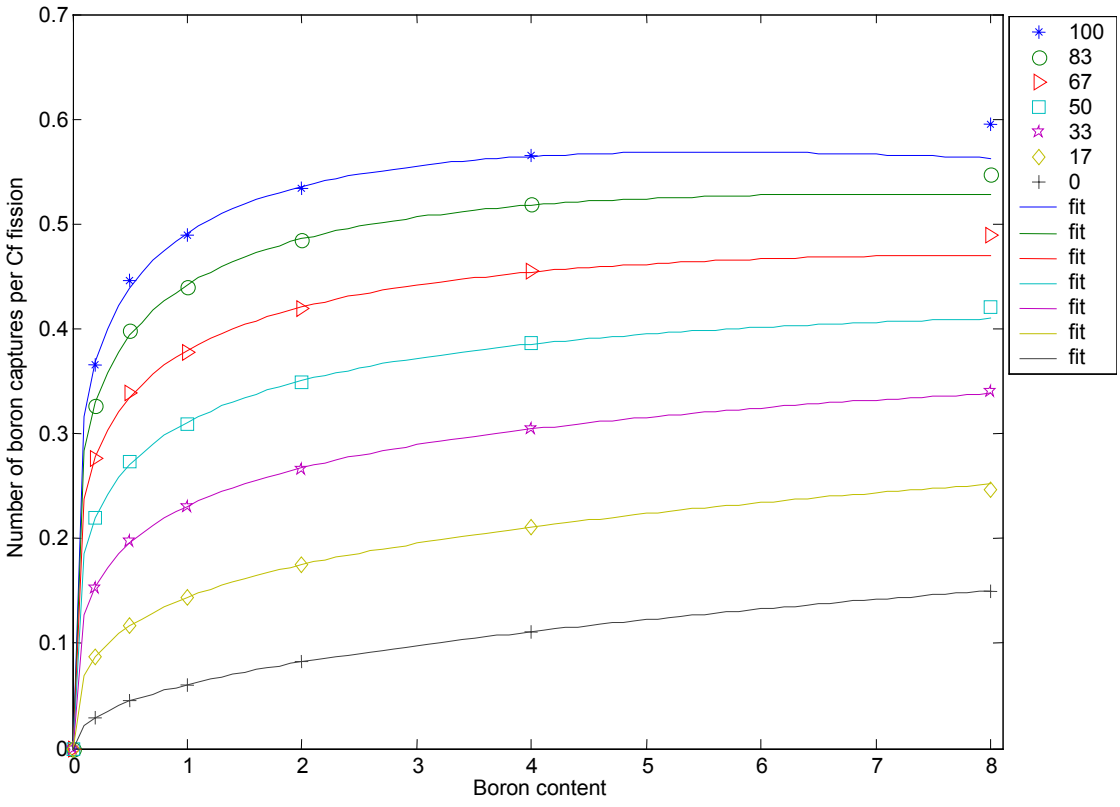

Fig. 4.4.4. Fit given by Eq. 4.4.1 to data from Fig. 4.4.2 for varying water content.

The procedure outlined in this section is based on calculated data. The procedure can be analogously applied to measured data. The extension of this procedure to the RCSBs requires the collection of further experimental data, which can be combined with Monte Carlo-generated sensitivity to B_4C content. This will have to be done with the detector explicitly in the calculations.

4.5 SUMMARY OF GAMMA RAY SPECTROMETRY

Boron peak counts are a function of both boron and hydrogen content. PGNAA measurements provide clear and easily recognizable evidence of the presence of boron in BoroBond™ material. Boron was detected in all sample blocks prior to baking. After bake-out, boron was detected in 2.3, 4.6, and 9.1 percent boron blocks but not in the nominal 0 percent blocks. Measured results became insensitive to BoroBond™ thickness at approximately 6 in., as evidenced by the asymptotic behavior of boron capture counts for all boron compositions. Given the liner model of section 4.2 wt% B_4C can be estimated to ± 1%.

Assuming that the water content is the same, PGNAA measurements using the RCSB indicated approximately 4 ± 1 wt% B_4C using data from points opposite approximately 6 in. of BoroBond™ material and the data from the blocks. It should be noted that the block results require small temporal corrections to account for the decay of ^{252}Cf but can be avoided by the use of an AmBe source for gamma ray spectrometry measurements.

The gamma peak due to hydrogen neutron capture was clearly observable and recognized by the Maestro analysis software in the unbaked blocks with 0 and 2 percent boron. The hydrogen peak was observable but not recognized by the Maestro software for baked blocks with 0 percent boron composition. Other block, unbaked and baked, and mockup RCSB measurements did not provide hydrogen peaks that could be recognized by the Maestro software. Based on these measurements, gamma spectrometry measurements would not be useful for the determination of hydrogen content in RCSBs with nominal boron concentration of 4 percent.

Measurements of gammas produced by inelastic scattering varied widely for blocks of the same nominal composition and thickness. Either actual variations in block compositions or insufficient counting times provided results that appear to be of little practical use.

5. PROPOSED VERIFICATION OF WATER AND B_4C CONTENT OF RCSBs

The recommended method to quantify the water content of the RCSBs is the fast neutron time-of-flight transmission method. Knowing the water content, the B_4C content will be obtained from the gamma ray spectrometry method, which is preferred over thermal neutron counting because it measures the gamma rays produced in boron capture. The fast neutron time-of-flight transmission and gamma ray spectrometry methods would be

implemented as follows. The data will also be used to assess the uniformity of the BoroBond™ in the RCSB and archived for future comparisons.

5.1 FAST NEUTRON TIME-OF-FLIGHT TRANSMISSION

This method uses two ^{252}Cf sources in ionization chambers inserted in two specially provided 6-in.-deep holes, each equidistant from four fissile storage can locations in the RCSB. Each fissile storage can location would contain one of six fast plastic scintillation detectors connected by cables to the associated electronics. A sketch of this configuration looking down on the RCSB is given in Fig. 5.1.1. A photograph of a measurement with the special mockup of the RCSB is given in Fig. 2.4.3 with only one Cf source in the left source hole (A) and a single detector in one fissile can storage location (4). (In the actual verification measurements the RCSB would not be standing on its side, but the bottom of the RCSB will be 3 ft. above the floor to minimize floor reflection effects.) The symmetry of the source detector arrangement allows easy assessment of the uniformity of the BoroBond™ material in the RCSB.

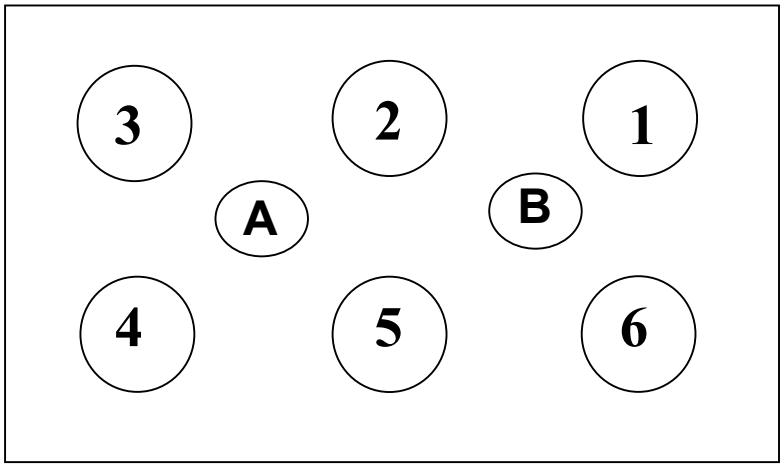

Fig. 5.1. Sketch of RCSB, top view (source locations A&B, fissile storage locations 1-6).

The ^{252}Cf source initial mass would be 0.5 micrograms (total dose of about 1 mrem/hr at one meter) and result in a measurement time of 15 minutes. These two sources would not have to be replaced for the at-the-factory determinations of water content of the RCSBs, because after three years the source intensity is decreased slightly more than a factor of two. Since the RCSB is an excellent neutron shielding material, the sources and detectors for this hydrogen content determination could be stored in a RCSB especially for this purpose when not in use for verification of the water content of the RCSBs.

5.2 GAMMA RAY SPECTROMETRY

Although the exploratory studies at ORNL used an HPGe gamma ray detector (with liquid nitrogen cooling) with high energy resolution, it is recommended that a lower resolution NaI (cheaper and room temperature) gamma ray detector be used for the at-the-factory measurements. Further evaluations should be performed to confirm this capability

for NaI. A sketch of the recommended configuration for gamma ray spectrometry is given in Fig. 4.2.1 with the block of the figure replaced with the sides of the RCSB. A 4-in. rectangular block of tungsten alloy between the source and the detector is required to reduce the direct response of the detector to the source. So as to not have to correct for the decay of the source, it is recommended to use an AmBe source (433 year half life) that could later be used at Y-12 if desirable (use of this source will have to be verified before implementation). With the water content determined from the fast neutron transmission, gamma ray spectrometry can be used to quantify the B_4C content.

6. STEPS IN AT-THE-FACTORY VERIFICATION OF RCSBS

This section briefly describes the steps in the at-the-factory-measurement. This is not intended to be a QA procedure for at-the-factory measurements. This QA procedure will have to be jointly drafted by Y-12 and Eagle-Picher with input from ORNL. The following are the basic steps in the procedure and assumes an apparatus exists for holding the 2 sources and 6 detectors for the fast neutron time-of-flight transmission measurement, and that the sources and detectors are stored on this fixture in a special RCSB for that purpose. It assumes that the gamma ray spectrometry measurement equipment is on a rollup cart that can place the equipment adjacent to the RCSB. It also assumes that the front neutron shield of the source can be rotated upward and back exposing the neutron source, tungsten block, and gamma detector so that they can be placed adjacent the RCSB. It also assumes that a user-friendly system exists with automated analysis so that it could be operated by a non-technical person.

Table 6.1. Steps in the RCSB Verification procedure for RCSBs

1. Turn on the computer system and operator hits start (this action turns on all power supplies to their nominal values). The computer responds when this is complete.
2. After the operator has allowed the system to warm up for four hours, he initiates the set up of detection system electronics.
3. The software adjusts Cf source channel electronics to proper values and then instructs the operator to raise the apparatus with the sources and detectors three feet above the storage pallet. The computer then makes the final adjustments of the electronics using the NMIS processor.
4. The computer then prompts the operator to install the sources and detectors into the RCSB to be verified. The operator enters the identifying number of the RCSB when this is done.
5. The computer starts the verification of the water content.
6. After completion (15 minutes), the water content is displayed on the terminal screen. An assessment of the uniformity of the BoroBond™ in the RCSB is also displayed on the terminal screen. All data is stored with the RCSB identifying number. The computer prompts the operator to return the apparatus with the sources and detectors to storage and to prepare for the gamma ray spectrometry measurement.

7. The operator rotates the front of the neutron shield upward and back exposing the neutron source,[‡‡] tungsten alloy block, and NaI detector of the gamma ray spectrometry system which is on a movable cart.
8 The computer instructs the operator to position the system adjacent to one end of the RCSB and lock the cart in place.
9. After positioning the operator prompts the computer to start the measurement.
10 When measurement is finished (20 minutes), computer prompts the operator to position the system at the other end of the RCSB and start another measurement.
11. After 20 minutes of data acquisition, the computer processes both sets of data knowing the water content from Step 6, and prints the weight percent B_4C from each measurement and the average.
12. The computer then displays a red or green indicator on the screen (green if wt% B_4C above or equal 4%), stores data and the result appropriately, and prompts the operator to remove the gamma ray spectrometry equipment.
13. If no more RCSBs are to be measured, the operator instructs the computer to turn the measurement system off. Otherwise, return to Step 4 for measurement of the next RCSB.

7. CONCLUSIONS

Extensive measurements at the Oak Ridge National Laboratory (ORNL) with BoroBond™ blocks of varying thickness, natural boron carbide (B_4C) content, and water content, and with a simplified mockup of the Rackable Can Storage Box (RCSB) of fixed natural B_4C and water content, have led to a method of quantifying the water content of RCSBs by fast neutron time-of-flight transmission measurements (NMIS)[§§] and quantifying the B_4C content with gamma ray spectrometry assuming the water content is known. The time-of-flight transmission measurements results can be used to assess the uniformity of the BoroBond™ in the RCSB. The data from both measurements will be stored for future comparisons to initial measurements. These methods can be implemented at the RCSB production site, or subsequently at the Y-12 National Security Complex during the operating lifetime of the RCSBs at the Highly Enriched Uranium Materials Facility.

REFERENCES

1. E. Padovani and S.A. Pozzi, "MCNP-PoliMi ver. 1.0. User's Manual", CESNEF-021125 Library of Nucl. Eng. Dept., Polytechnic of Milan, Italy, Nov. 2002.

[‡‡] It is proposed to use a long half life AmBe neutron source, and this will have to be evaluated experimentally.
[§§] The time-of-flight transmission measurements utilized the Nuclear Materials Identification System (NMIS) with ^{252}Cf source. NMIS is the system for confirmation of receipts and inventories at HEUMF.

APPENDIX A. DETAILS OF THE MOCKUP RCSB AND BOROBOND™ MATERIALS

A1. DETAILS OF SPECIAL MOCKUP RCSB

A photograph of the special RCSBs for these measurements as the BoroBond™ was being added is given in Fig. A1. A sketch of the gusset locations in the test pour mold of Fig. A1 is given in Fig. A2. Some of the gussets between fissile storage locations are visible in Fig. A1.

Fig. A1. Test pour for the mockup RCSB on January 31, 2002 at Eagle-Picher Facilities.

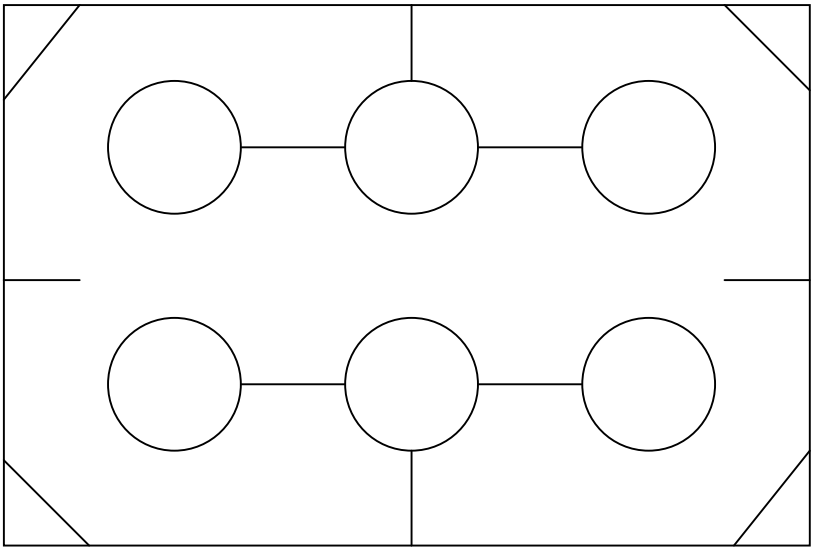

Fig. A2. Gusset and fixed storage locations in test pour mold (not to scale).

A2. BOROBOND™ MATERIAL

BoroBond™ is based on an exothermic chemical reaction between relatively pure forms of MgO, KH_2PO_4, and H_2O at room temperature to produce a chemically bonded, phosphate-based ceramic solid known as MKP:

$$MgO\ (powder) + KH_2PO_4\ (powder) + 5\ H_2O\ (liquid) \rightarrow MgKPO_4{\cdot}6\ H_2O\ (solid)$$

The incorporation of fly ash and B_4C powder results in a cost-effective neutron-absorbing medium that can accommodate a broad variety of compositions.

The mixing compositions of the BoroBond™ blocks for various B_4C contents are given in Table A1. The fly-ash and B_4C content was adjusted to produce the various B_4C content blocks. The amount of MgO, KH_2PO_4, and H_2O were the same for all block compositions. The composition of the fly-ash used for the BoroBond™ blocks is given in Table A2. The isotopic analysis of the Boron is given in Table A3 and the expected densities are given in Table A4. These values of Table A4 are higher than actual, refer to Tables B6 and B7, due to incorporation of air in casting of blocks or loss of water.

Table A1. Mix-proportions in wt% from Eagle-Picher on June 13, 2002 for BoroBond™ blocks

	Composition A	**Composition** B	**Composition** C	**Composition** D
Weight % MgO	10.49	10.49	10.49	10.49
Weight % KH_2PO_4	32.20	32.20	32.20	32.20
Weight % H_2O	21.33	21.33	21.33	21.33
Weight % Fly Ash	35.98	33.70	31.42	26.86
Weight % $^{nat}B_4C$	0.00	2.28	4.56	9.12

Table A2. Fly-ash composition from Eagle-Picher on September 26, 2002 for BoroBond™ blocks

Constituent	**Weight %**
Al_2O_3	28.47
CaO	2.70
Fe_2O_3	13.87
K_2O	1.76
MgO	0.95
Na_2O	0.30
P_2O_5	0.13
SO_3	0.50
SiO_2	50.00
unaccounted	1.32
Total	**100.00**

Table A3. Boron carbide specifications from Eagle-Picher on September 26, 2002 for BoroBond™ blocks

Property	Weight %
Total B	74.89
^{10}B/B ratio	18.40
^{11}B/B ratio	81.60
Total C	22.64
unaccounted	2.47

Table A4. Density estimates for "as-cast" blocks from Eagle –Picher for BoroBond™ blocks

	Composition A	**Composition** B	**Composition** C	**Composition** D
Density (g/cm^3)	1.910	1.922	1.919	1.913

The densities of the blocks during the measurements were less than these due to loss of water to the ambient air (refer to Tables B6 and B7).

APPENDIX B: MISCELLANEOUS MEASUREMENT DETAILS

B1. BAKE-OUT OF BOROBOND™ BLOCKS

Four sets of test blocks, with 8 blocks in each set, of various boron concentration and thickness were provided in order to investigate boron and water content sensitivity as a function of boron and/or water content and block thickness. After an initial set of gamma spectroscopy and fast transmission measurements, half of the blocks, the even numbered blocks were baked at 140°C for approximately 24 hours in order to reduce the water content to ~5/6 of the original value and thus, vary the water content.

Methodology

This investigation initially considered baking the blocks to 400°C in order to remove all hydrogen (in the form of water) from the blocks. A small sample block of the BoroBond™ material, 47x97x165 mm, was baked out with the bake-out schedule provided in Table B1. Temperatures were measured with thermocouples in the blocks. Oven heat-up and cool-down were automatically controlled.

Table B1. Bake-out schedule for small sample block

Temperature range (°C)	Heat-up rate (°C/h)
Ambient-200	30
200-400	60
400	24 hour bake
400-200	60
200-Ambient	30

The sample block mass was 1434 g prior to bake-out and 1089 g after bakeout, a change of 24.2% due to removal of water. Table B2 presents sample block mass measurements prior to and after bakeout. Note that after bakeout, water is absorbed from the ambient air resulting in a weight increase with time.

Table B2. Sample block mass measurements

Date	Mass (g)
7/17/2002	1434
7/30/2002	1089
8/1/2002	1091
8/7/2002	1092
8/20/2002	1092

While the bake-out of the sample block was successful in terms of removing water from the block, the structural integrity of the sample block appeared to be severely

weakened. Figure B1 shows the sample block after bake-out. Note the severe surface cracking of the block.

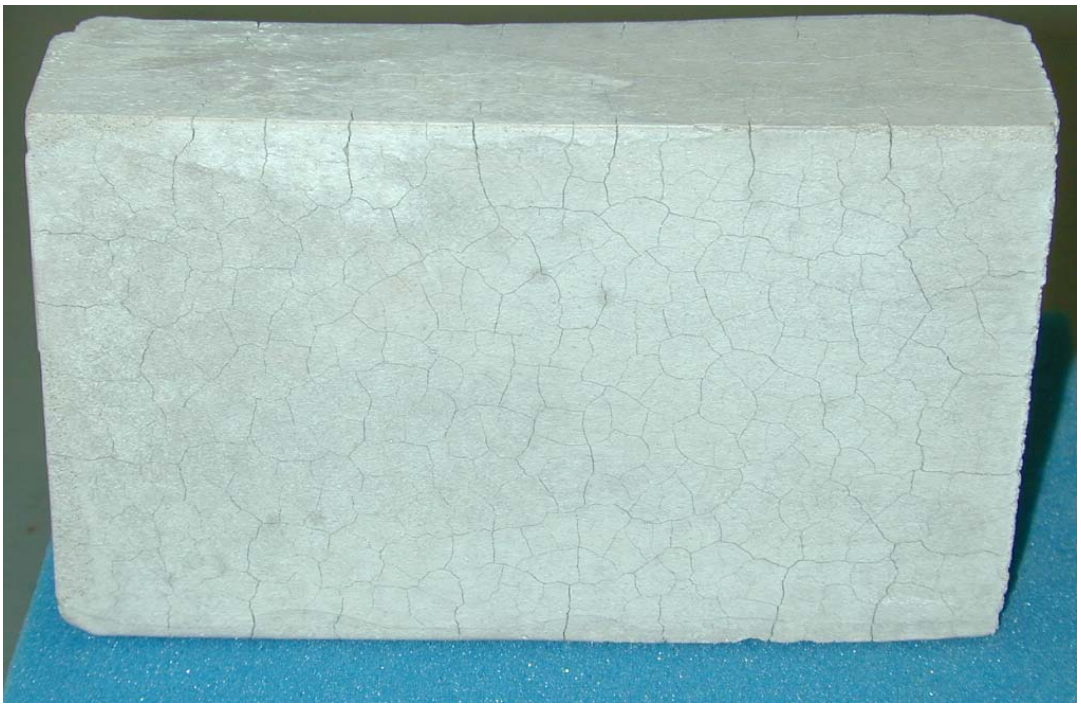

Figure B1. Sample block after bake-out.

Even with careful handling of the sample block, pieces were easily chipped from the block. After further consideration, it was decided to bake out the test blocks to 140°C in order to remove ~5/6 of the water in the blocks. Table B3 provides the bake-out schedule for the test blocks.

Table B3. Bake-out schedule for test blocks

Temperature range (°C)	Heat-up rate (°C/h)
Ambient-140	30
140	24 hour bake
140-Ambient	30

Bake-out removed an average of 19.3% of the mass in the blocks with a variation of 18 to 20.4%. Table B4 presents the mass of the blocks just before and after bakeout and the mass loss of baked out blocks. Baking to 140°C resulted in adequate structural integrity for the test blocks with significantly less chipping than that observed for the sample block described above. These values are not quite the 21.3 wt% of Table A2 since the blocks have lost some water between initial production and bakeout.

Table B4. Masses of blocks immediately before and after baking

Block ID	Pre-bake mass (g)	Post-bake mass (g)	Mass loss (%)[a]
A2	17556	14197	19.1
A4	17518	14140	19.3
A6	8914	7193	19.3
A8	8474	6834	19.4
B2	17375	14240	18.0
B4	17619	14230	20.0
B6	8919	7167	20.4
B8	8884	7183	19.1
C2	17657	14236	20.3
C4	17632	14285	18.7
C6	8870	7156	19.1
C8	8641	6959	20.2
D2	17578	14223	19.1
D4	17544	14249	18.8
D6	8615	6973	19.1
D8	8528	6899	19.1

[a]Reduction in water content.

B2. CHANGES IN BLOCK MASS WITH TIME

Changes in block masses over time were noted since receipt of the test blocks. Prior to bake-out, the mass of all blocks decreased over time. This is a result of excess water in the blocks originally. The mass change was almost 3% in a three-month time period. After bake-out, the mass of all baked blocks increased over time due to absorption of water from ambient air. Table B5 provides mass data for all blocks at various times. A mass versus time curve can be generated for each block. Since the RCSBs will be canned in steel, a similar change in mass of the RCSBs should not be expected.

B3. DIMENSIONS OF BOROBOND™ BLOCKS

The dimensions of the BoroBond™ blocks are given in Table B6. These values were used to obtain the densities of the individual blocks which are summarized in Table B7. The 2-in.-thick blocks have higher densities than the 4-in.-thick blocks in all cases both before and after bakeout presumably due to less inclusion of air in casting. All densities in Table B7 are lower than those of Table A4.

B4. RESULTS OF NEUTRON COUNTING MEASURMENTS

The measured neutron counting rates from the bare detector (#1 thermal plus epithermal neutrons), the cadmium covered detector (#2 epithermal neutrons), and the difference (thermal neutrons) are given in Table B8 for various B_4C and water contents.

B5. MEASURMENT DATES

Table B9 provides dates for each of the measurement methods.

Table B5. Weights of BoroBond™ blocks on various dates in 2002[a]

Block ID	7/25	8/12	9/9	9/10	9/12	9/16	9/17	9/18	9/20	9/21	9/23	9/30	10/14	10/21
A1	17772	17648		17535	17527		17514	17512	17503			17486	17453	17427
A2	17793	17671	17556				14197	14232	14252			14283	14318	14321
A3	17696	17581		17475			17451	17448	17444			17429	17396	17371
A4	17758	17625	17518				14140	14175	14198			14236	14278	14283
A5	8567	8507		8460			8448	8447	8445			8439	8426	8415
A6	9001	8939	8914				7193	7223	7232			7257	7276	7279
A7	9024	8957		8905			8893	8892	8891			8884	8868	8855
A8	8553	8499	8474				6834	6864	6874			6898	6918	6921
B1	17788	17610		17462					17402			17392	17352	17323
B2	17685	17517	17375			14240			14261			14304	14320	14318
B3	17687	17506		17376					17309			17297	17256	17225
B4	17803	17619	14230	14247		14278			14288			14316	14343	14342
B5	8977	8902		8854					8828			8828	8813	8800
B6	9000	8919	7167	7181		7200			7207			7227	7277	7277
B7	8987	8918		8882					8849			8849	8842	8822
B8	9015	8935	8884			7183			7227			7252	7265	7267
C1	17900	17691		17538				17526		17508		17483	17441	17415
C2	17873	17657	14236	14255				14277		14273		14346	14364	14363
C3	17860	17655		17492				17467		17450		17425	17381	17353
C4[b]	17884	17681		14333				14344		14344		14413	14425	14423
C5	8949	8861		8803				8800		8794		8787	8772	8761
C6[c]	8976	8889		7186				7191		7191		7253	7257	7256
C7	8780	8695		8638				8636		8629		8623	8610	8599
C8	8721	8641	6959	6976				6986		6988		7049	7056	7056
D1	17996	17765		17632	17625					17598	17590	17581	17562	17528
D2	17942	17711		17578						14223	14252	14326	14340	14339
D3	17899	17664		17524	17516					17486	17479	17467	17448	17413
D4	17926	17683		17544						14249	14277	14332	14361	14362
D5	8778	8662		8611	8607					8593	8592	8589	8585	8567
D6	8799	8670		8615						6973	6993	7020	7042	7044
D7	8673	8547		8490	8486					8475	8473	8469	8464	8448
D8	8710	8585		8528						6899	6918	6942	6959	6964

[a]Where weights change by ~20% between columns the blocks have been baked out. Values immediately before and after bakeout are given in Table B4.
[b]Block C4 had a weight of 14306 on 8/30 and 14320 on 9/4.
[c]Block C6 had a weight of 7167 on 8/30 and 7177 on 9/4.

Table B6. Measured dimensions, weights, and densities of BoroBond™ blocks on September 20, 2002

Block ID	Measured dimensions at various locations (mm)[a]												Average dimension (mm			Weight (gms)	Density[b] (g/cm^3)
	1	2	3	4	5	6	7	8	A	B	C	D	Thick	Lengtha avg	Width avg	9/20/02	Density
A1	101.98	101.99	101.87	101.85	101.99	101.96	102.01	101.99	307.53	307.58	307.32	307.41	101.96	307.43	307. 05	17503	1.8160
A2	101.91	101.87	102.00	101.84	101.90	101.94	101.91	101.95	306.46	307.3	306.12	307.37	101.92	306.29	307.34	14252	1.4856
A3	101.39	101.41	101.53	101.37	101.35	101.50	101.41	101.45	306.87	307.49	306.88	307.57	101.43	306.88	307.53	17444	1.8224
A4	101.94	101.91	101.99	101.98	101.89	101.92	101.87	101.93	306.33	307.74	306.68	307.56	101.93	306.51	307.65	14198	1.4772
A5	48.59	48.6	48.68	48.64	48.67	48.60	48.51	48.60	306.16	305.07	306.96	306.37	48.61	306.56	305.72	8445	1.8536
A6	50.93	50.94	50.92	50.94	50.97	50.97	50.98	50.95	306.14	306.18	305.44	306.53	50.95	305.79	306.36	7232	1.5152
A7	50.96	51.01	50.97	51.19	51.18	50.98	50.94	50.95	305.91	306.45	305.21	306.55	51.02	305.56	306.5	8891	1.8606
A8	48.38	48.48	48.38	48.42	48.42	48.37	48.37	48.40	306.29	305.60	305.60	305.72	48.40	305.95	305.66	6874	1.5187
B1	102.35	101.83	101.94	101.85	101.88	101.92	101.96	101.92	307.30	307.75	308.05	307.82	101.96	307.67	307.79	17402	1.8024
B2	101.9	101.83	101.8	101.86	101.82	101.92	101.85	101.73	305.88	307.46	306.41	307.47	101.84	306.15	307.47	14261	1.4877
B3	101.91	101.90	101.88	101.88	101.96	101.70	101.78	101.77	306.64	307.58	306.44	307.39	101.85	306.54	307.49	17309	1.8031
B4	101.67	101.76	101.6	101.61	101.61	101.58	101.61	101.60	306.14	306.94	306.28	307.23	101.63	306.21	307.09	14288	1.4951
B5	50.95	50.94	50.95	50.95	50.95	50.94	50.93	51.02	307.19	305.84	307.62	307.32	50.95	307.40	306.58	8828	1.8384
B6	50.81	50.85	50.97	50.91	50.81	50.89	50.81	50.85	307.78	306.70	307.28	306.36	50.86	307.53	306.53	7207	1.5031
B7	50.90	50.88	50.88	50.97	50.90	50.92	51.00	51.05	305.55	307.71	306.79	307.61	50.94	306.17	307.66	8849	1.8443
B8	50.85	50.82	50.89	50.83	50.84	50.87	50.85	50.88	306.52	306.52	307.25	306.23	50.85	306.88	306.38	7227	1.5115
C1	101.95	101.93	101.94	101.97	101.90	101.90	101.96	101.91	306.75	307.74	307.35	307.85	101.93	307.05	307.80	17508	1.8174
C2	101.84	101.82	101.76	101.76	101.85	101.66	101.71	101.72	305.69	306.92	306.05	306.85	101.76	305.87	306.89	14273	1.4942
C3	101.98	101.91	101.98	101.96	101.93	101.98	102.18	101.93	306.29	307.07	306.35	307.23	101.98	306.32	307.15	17450	1.8190
C4	101.80	101.77	101.84	101.78	101.80	101.79	101.82	101.88	305.95	306.76	306.26	306.85	101.81	306.11	306.81	14344	1.5002
C5	50.72	50.70	50.68	50.61	50.64	50.64	50.63	50.76	307.40	306.80	305.65	307.04	50.67	306.53	306.92	8794	1.8447
C6	50.49	50.55	50.50	50.57	50.57	50.56	50.57	50.69	306.19	307.34	306.52	307.04	50.56	306.36	307.19	7191	1.5112
C7	49.68	49.74	49.72	49.66	49.71	49.67	49.67	49.67	305.88	307.15	306.53	307.23	49.69	306.21	307.19	8629	1.8462
C8	48.90	49.03	48.99	49.06	49.06	49.04	49.02	49.07	305.98	306.86	305.73	306.60	49.02	305.86	306.73	6988	1.5195
D1	101.98	101.99	101.97	101.99	101.98	101.95	102.01	101.96	307.46	308.57	308.17	308.58	101.98	307.82	308.58	17598	1.8168
D2	101.88	101.81	101.88	101.76	101.86	101.87	101.92	101.82	306.48	307.78	307.07	307.57	101.85	306.78	307.68	14223	1.480
D3	101.92	101.99	101.95	101.86	101.86	101.88	101.94	101.91	306.67	307.82	306.94	307.6	101.91	306.81	307.71	17486	1.8174
D4	101.86	101.88	101.82	101.88	101.87	101.82	101.73	101.69	306.32	307.32	306.25	307.34	101.82	306.29	307.33	14249	1.4867
D5	49.50	49.52	49.54	49.48	49.5	49.57	49.44	49.49	307.06	305.86	307.27	307.76	49.505	307.17	306.81	8593	1.8419
D6	49.53	49.61	49.55	49.51	49.51	49.53	49.54	49.57	306.64	307.67	306.66	307.98	49.544	306.65	307.83	6973	1.4910
D7	48.82	48.82	48.85	48.83	48.82	48.87	48.74	48.85	306.19	307.76	307.17	307.96	48.825	306.68	307.86	8475	1.8385
D8	49.03	48.94	48.86	48.80	48.84	48.91	48.83	48.86	306.76	307.95	306.63	307.5	48.884	306.70	307.73	6899	1.4954

[a]Locations 1-8 for thickness were 3 in. in from the corners and 2 in. in from the center of each side. Locations A, B, C, and D were the four side lengths of the blocks.
[b]Densities calculated from average length, width, and weight.

Table B7. Densities of BoroBond™ blocks on September 20, 2002

Block number	Densities (g/cm^3) for series[a]			
	A	B	C	D
1	1.8160	1.8024	1.8174	1.8168
2	1.4856	1.4877	1.4942	1.4795
3	1.8224	1.8031	1.8187	1.8174
4	1.4772	1.4951	1.5002	1.4867
5	1.8536	1.8384	1.8447	1.8419
6	1.5152	1.5031	1.5112	1.4910
7	1.8606	1.8443	1.8462	1.8385
8	1.5187	1.5115	1.5195	1.4954

[a]After bakeout for even numbered blocks.

Table B8. Measured neutron count rate for varying B_4C and water content blocks[a]

Block number[b]	Thickness (inches)	Measurement time	Average Count Rates (cps) Detector 1 (total)	Detector 2[c] (epithermal)	Difference[d] (thermal)
A5	2	150	8638	2759	5878
A6	2	500	292	256	35.78
A1	4	300	14767	2772	11995
A2	4	300	787	528	258
A1,A5	6	300	10966	1598	9367
A2,A6	6	300	1030	549	481
A1,A3	8	300	5975	703	5271
A2,A4	8	400	1037	488	549
A1,A3,A5	10	600	2736	312	2423
A2,A4,A6	10	600	930	389	541
A1,A3,A5,A7	12	600	1168	137	1031
A2,A4,A6,A8	12	600	385	146	239.4
B5	2	150	2563	2003	560
B6	2	150	486	474	11.46
B1	4	200	2321	1681	638
B2	4	300	424	406	17.7
B1,B5	6	300	1324	914	409.7
B2,B6	6	300	353	333	20.0
B1,B3	8	300	586	425	160.8
B2,B4	8	300	267	252	14.84
B1,B3,B5	10	300	268	185	83.22
B2,B4,B6	10	300	191	176	14.87
B1,B3,B5,B7	12	600	116	81	35.2
B2,B4,B6,B8	12	600	129	121	8.75
C5	2	150	1794	1630	164
C6	2	350	239	228	11.0
C1	4	300	1412	1237	175
C2	4	400	368	339	29.6
C1,C5	6	300	759	639	121.8
C2,C6	6	300	280	273	6.34
C1,C3	8	300	327	281	46.2
C2,C4	8	300	194	188	5.78
C1,C3,C5	10	300	147	124	22.2
C2,C4,C6	10	300	135	129	6.78
C1,C3,C5,C7	12	600	67	56	10.3
C2,C4,C6,C8	12	500	45.65	44	0.92
D5	2	150	1258	1207	50.92
D6	2	150	441	439	1.56
D1	4	150	890	804	86.06
D2	4	300	310	305	5.55
D1,D5	6	300	424	393	30.91
D2,D6	6	300	217.1	207	10.22
D1,D3	8	300	175.7	163	12.53
D2,D4	8	300	139.2	134	5.66
D1,D3,D5	10	500	40.4	37	3.07
D2,D4,D6	10	300	90.7	87	3.57
D1,D3,D5,D7	12	600	39.7	35	4.24
D2,D4,D6,D8	12	600	57.5	57	0.96

[a]Measurements performed on September 28, 2002.
[b]Even numbered blocks were baked to remove 5/6 of water.
[c]Detector 2 was covered with cadmium so it detected epithermal neutrons above the Cd cut off energy (0.5 ev).
[d]Difference represents thermal neutrons below the Cd cut off energy of 0.5 ev.

Table B9. Measurement dates

Gamma spectroscopy measurements

	Unbaked	Baked
A block	7/18/02	9/17/02
B block	7/20/02	9/16-9/17
C block	8/5/02-8/6/02	9/9-9/10
D block	8/7/02	9/23

Neutron transmission measurements

	Unbaked	Baked
A block	7/30-8/1	9/19/02
B block	7/30-8/1	9/20/02
C block	7/30-8/1	9/22/02
D block	7/30-8/1	9/23/02

Neutron Counting Measurements
All 9/28/02

APPENDIX C. Cf SOURCE INTENSITIES TRACEABLE TO NIST

The ^{252}Cf sources are calibrated against a NIST secondary calibration source which is traceable to a NIST primary ^{252}Cf calibration source. Source NSS19 was utilized as a calibration standard which was originally compared to a secondary calibration source at ORNL for ^{252}Cf mass determination. We receive a monthly certification of the number of micrograms of ^{252}Cf in this source. From the isotopic analysis of the other isotopes of californium in the sources at the time of fabrication and the known half lives of ^{250}Cf and ^{252}Cf the neutron output of NSS19 can be obtained and was 3.623×10^5 on October 18, 2002. The isotopic analyses are given in Table C1. The other main contributor to the neutron output is ^{250}Cf which produces for source NSS19 ~ 30 % of the neutrons on October 18, 2002.

Relative neutron counting measurements were performed with three polyethylene moderated 2-in.-thick, 10.4-in.-active length ^{3}He proportional counters spaced approximately 2 or more feet from the source. This large distance was used to make the measurement insensitive to precise location of the sources. The distance was also chosen to assure that the count rate in the proportional counter was below 5000 counts per second for the largest Cf source (Cf 44) to avoid dead time effects. Background count rates from cosmic ray neutrons were measured and found to be negligible <0.5 cps. In these measurements, Cf 44 and Cf 21, which are a Cf ionization chamber and the six pellet sources, were measured relative to NSS19. Cf 21, although not used in the block or mockup RCSB measurements, was measured as a consistency check. The average relative count rates and neutron intensities are given in Table C2.

To check the validity of the correction for half life and isotopic analysis, the neutron output of Cf-21 was calculated from the initial ^{252}Cf content and isotopic analysis in 1983 when the source was fabricated. It was within 2.2% of that given in Table C2.

Table C1. Isotopic analysis of Cf source

	Isotopics[a] of Cf source from mass spectrographic analysis (atm %)		
Isotopic	**21 (3/24/83)**	**44 (3/8/01)**	**NN19 (7/13/70)**
249	17.44	2.72	1.048
250	7.56	9.10	9.69
251	2.14	2.75	2.77
252	72.82	85.05	86.43
253	0.08	0.38	0.045
254	0.05	0	0.014

[a]Dates of isotopic analysis are given in parenthesis.

Table C2. Ratio of neutron intensities for Cf source relative to NSS19 and neutron source intensities

Source ID	Relative neutron counting	Neutron output on Oct. 18, 2002
21[a]	0.497	1.803 E5
6 pellets	5.355	1.940 E6
44[a]	10.864	3.936 E6

[a]Both in ionization chambers.

Thus, count rate ratios to NSS19 determine the absolute neutron intensity of the six pellet and Cf 44 sources which are necessary in order to use the gamma ray spectrometry and neutron counting data to verify calculations.

A sketch of the configuration of Cf44 in an ionization chamber is given in Fig. C1. A sketch of the pellet sources is given in Fig. C2 and NSS19 in Fig. C3.

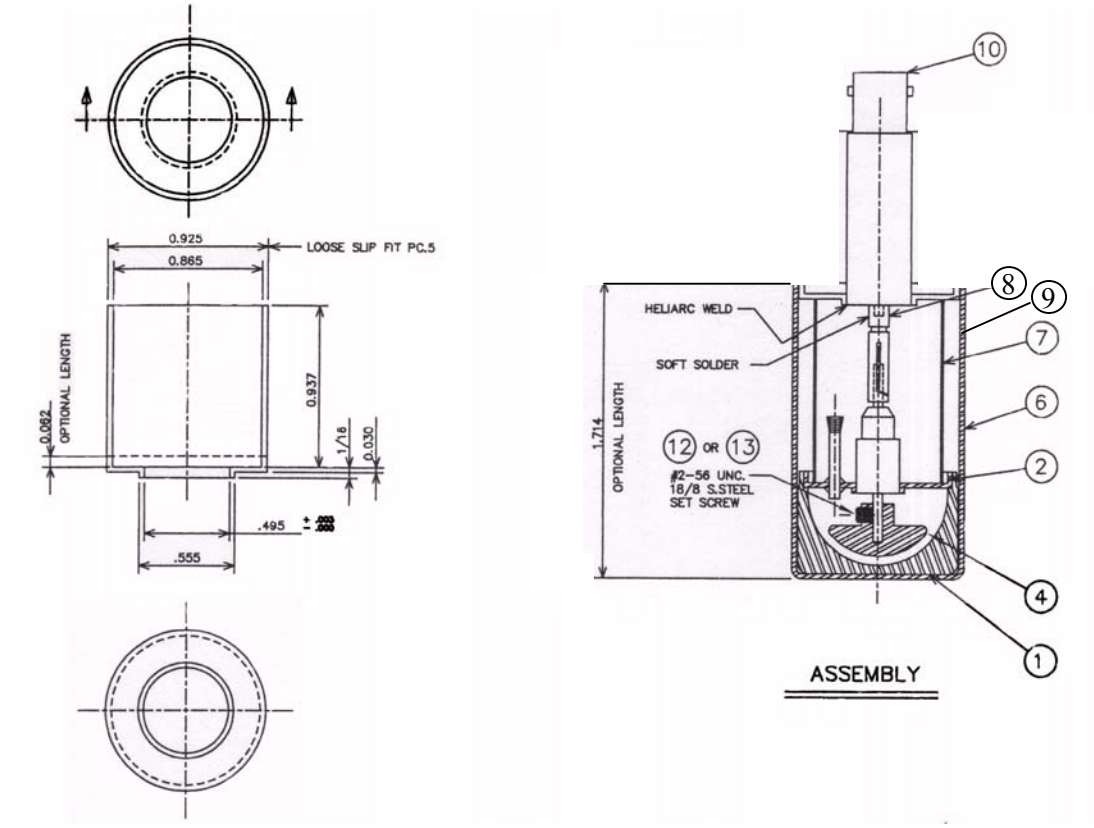

Fig. C1. Sketch of Cf 44 source ionization chamber.

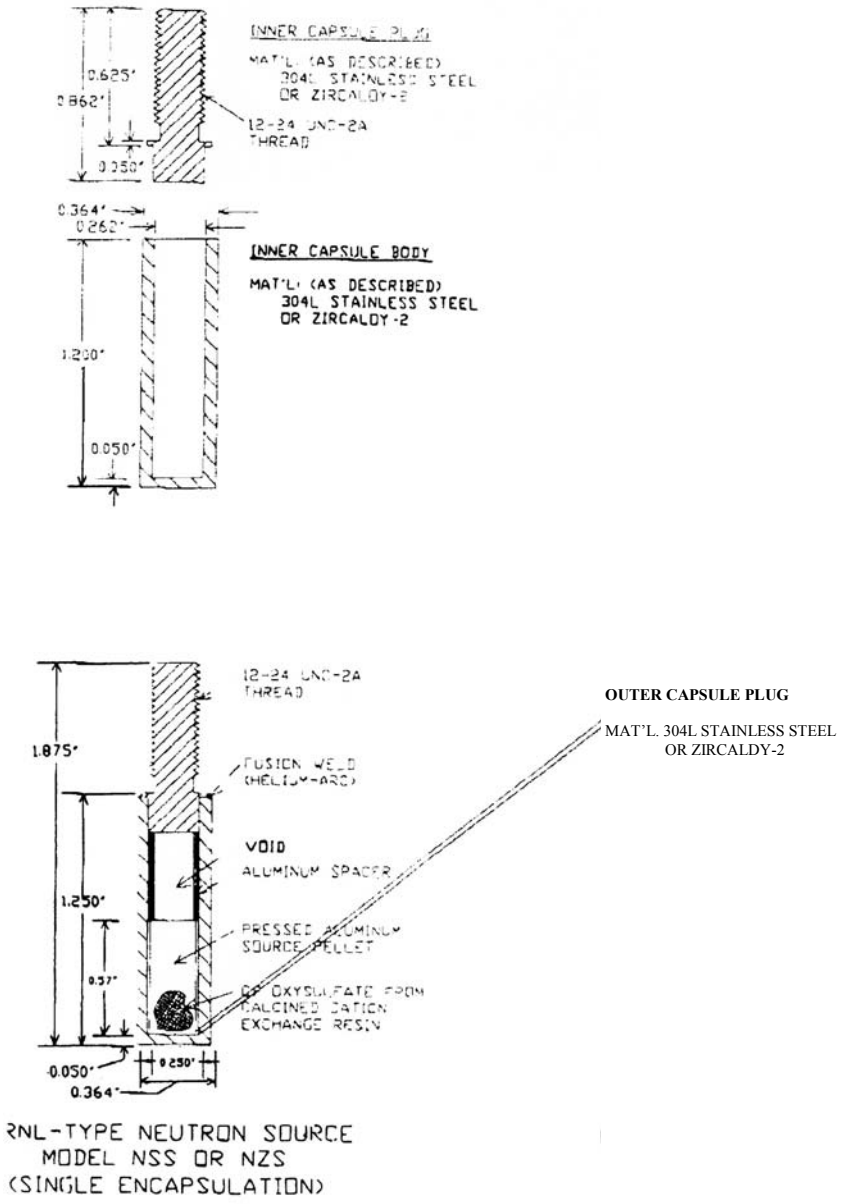

Fig. C2. Details of Cf source NSS19 encapsulation.

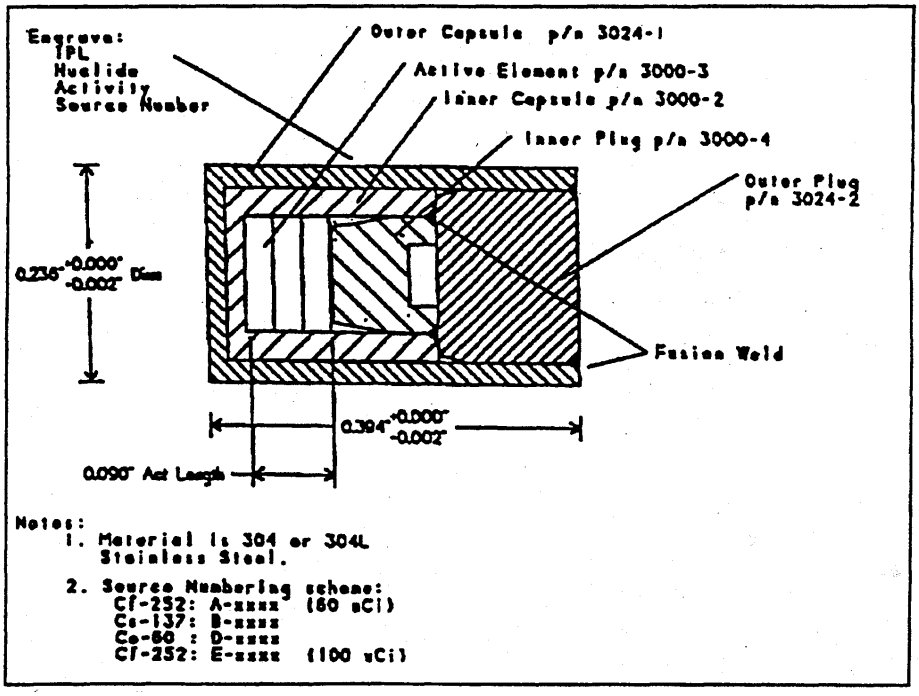

Fig. C3. Cross section sketch of pellet sources.

APPENDIX D. DETAILS OF GAMMA SPECTROMETRY MEASUREMENTS

ENERGY RESOLUTION VS. AMPLIFIER SHAPING TIME MEASUREMENTS

In order to understand the effects of amplifier shaping time on energy resolution a short study was conducted using four gamma lines, ^{137}Cs (662 keV), ^{60}Co (1173 keV), ^{60}Co (1332 keV), and ^{40}K (1460 keV). Spectra were taken for each source with amplifier shaping times of 2, 3, and 6 microseconds. Energy resolution in keV at Full Width Half Maximum (FWHM) and Full Width One-Fifth Maximum (FWOFM) values are presented in Table D1.

Table D1. Energy resolution as a function of amplifier shaping time

Shaping Time (microseconds)	FWHM/FWOFM ^{137}Cs (662 keV),	FWHM/FWOFM ^{60}Co (1173 keV)	FWHM/FWOFM ^{60}Co (1332 keV)	FWHM/FWOFM ^{40}K (1460 keV)
2	2.46/3.78	3.00/4.79	3.44/5.55	3.89/6.00
3	2.25/3.63	3.03/4.90	2.83/4.80	3.32/5.16
6	2.15/3.39	2.90/4.63	3.03/5.00	2.83/4.63

While energy resolution for 6 microsecond shaping time was consistently better than the resolution at 3 microseconds, it was decided to use a 3 microsecond shaping time since at higher count rates (as expected for our block and RCSB measurements) the longer shaping time of 6 microseconds would be offset by counting losses, pileup and baseline shift effects.

ENERGY RESOLUTION VS. APPLIED VOLTAGE MEASUREMENTS

Energy resolution for the detector and signal-processing electronics was investigated using several radioactive sources. Energy resolution for a HPGe detector may be understood as a combination of three factors: statistical spread in the number of charge carriers, variations in charge collection efficiency, and contributions of electronic noise. The statistical spread in the number of charge carriers is dictated by physics and the contributions of electronic noise were set by our choice of signal-processing electronics. The last effect to be considered, variations in charge collection efficiency, is usually a function of the applied voltage (and associated change in electric field). Measurements were made at several applied voltages (2000, 2800, 3000, 3200, 3400 V) for several gamma ray energies:^{137}Cs (662 keV), ^{54}Mn (835 keV), ^{22}Na (1275 keV), ^{60}Co (1173, 1333 keV). Results are presented in Table D2.

Table D2. Energy resolution as a function of applied voltage

Nuclide energy (keV)	Applied voltage (V)	FWHM (keV)	FWOFM (keV)
662	2000	-	-
662	2800	2.63	4.27
662	3000	2.58	4.30
662	3200	2.63	4.21
662	3400	2.53	4.04
835	2000	4.10	6.38
835	2800	3.23	5.20
835	3000	3.16	5.31
835	3200	3.33	5.40
835	3400	2.76	4.53
1275	2000	5.67	8.45
1275	2800	6.84	6.84
1275	3000	3.78	6.09
1275	3200	3.78	6.05
1275	3400	3.74	5.78
1173	2000	5.38	8.02
1173	2800	4.46	6.61
1173	3000	4.10	6.38
1173	3200	4.00	6.19
1173	3400	3.52	5.71
1333	2000	6.28	8.86
1333	2800	4.39	7.13
1333	3000	4.37	7.03
1333	3200	4.11	6.49
1333	3400	4.08	6.48

Energy resolution for all gamma energies was best at an applied voltage of 3400V. All measurements were performed at a detector bias voltage of 3400V.

REPRODUCIBILITY OF GAMMA SPECTROSCOPY MEASUREMENTS

In order to verify the reproducibility of measurements using our gamma spectroscopy equipment, a short study was conducted using a ^{137}Cs source placed 26.5 cm from the front face of the HPGe detector. Results are presented in Table D3.

Table D3. Reproducibility measurements using ^{137}Cs source

Measurement number	Counts	Std dev
1	4601	71
2	4506	70
3	4580	71
4	4538	71
5	4585	70
6	4556	69
7	4493	70
8	4553	70
9	4485	70
10	4593	71
11	4539	70
12	4428	70
13	4497	71
14	4397	69
15	4639	71
16	4579	70
17	4535	70

The variance-weighted estimator for these measurements is 4535 counts with a standard deviation of 17 counts. A chi-squared test of the data indicated that the individual measurements were compatible.

MEASUREMENTS RESULTS FOR BOROBOND™ BLOCKS

The results of the gamma spectrometry measurements are given in Table D4 where the number of counts in the boron peak for various combinations of blocks before baking are given. Similar results for the block after baking are given in Table D5. The average values are given in Table D6 before and after bakeout.

Table D4. Individual boron capture gamma ray measurements results for BoroBond™ blocks before baking

Block number	Nominal thickness (in.)	Integral counts $\nu \pm \sigma$ between 465 and 490 KeV for block series			
		A	B	C	D
5	2	10612 ± 432	92905 ± 547	98573 ± 536	110447 ± 543
6	2	10543 ± 444	87118 ± 535	99623 ± 540	109726 ± 544
7	2	12432 ± 444	88195 ± 535	95622 ± 529	107665 ± 536
8	2	10237 ± 460	89070 ± 527	93591 ± 529	109363 ± 538
1	4	35331 ± 529	185076 ± 676	188923 ± 655	208835 ± 677
3	4	37163 ± 550	179402 ± 666	191671 ± 667	204255 ± 672
2	4	37530 ± 551	188453 ± 679	193053 ± 671	207940 ± 677
4	4	37828 ± 554	187621 ± 688	189577± 661	206580 ± 672
5,7	4	42378 ± 554	197380 ± 687	194513 ± 670	206441 ± 673
6,8	4	37960 ± 553	184434 ± 668	194930 ± 667	204036 ± 671
1,5	6	48128 ± 568	208972 ± 704	211066 ± 685	229331 ± 700
2,6	6	49113 ± 594	213993 ± 714	215680 ± 699	228271 ± 704
1,3	8	50239 ± 601	211076 ± 709	212816 ± 688	231393 ± 706
2,4	8	50944 ± 603	215478 ± 721	218386 ± 701	232312 ± 706
1,3,5	10	44496 ± 564	212815 ± 710	214081 ± 688	232560 ± 709
2,4,6	10	51461 ± 606	216869 ± 722	220320 ± 698	231250 ± 707
1,3,5,7	12	45794 ± 563	210159 ± 714	213254 ± 690	231827 ± 706
2,4,6,8	12	52254 ± 620	216863 ± 722	218717 ± 701	230924 ± 707

Table D5. Average boron capture gamma ray measurements results for BoroBond™ blocks

Thickness (in.)	Average integral counts $\nu \pm \sigma$ in boron peak (465 keV to 490 keV) for series[a]						
	A[b]	B		C		D	
	Unbaked	Unbaked	Baked	Unbaked	Baked	Unbaked	Baked
2	10963 ± 222	89281 ± 268	7546 ± 305	96812 ± 267	12714 ± 302	109289 ± 270	21800 ± 321
4	37986 ± 224	186951 ± 276	18854 ± 278	192079 ± 272	30355 ± 281	206337 ± 275	49121 ± 304
6	48598 ± 412	211447 ± 501	29095 ± 503	213326 ± 489	40391 ± 515	228804 ± 496	64500 ± 559
8	50590 ± 426	213240 ± 506	32999 ± 509	215549 ± 491	45350 ± 524	231853 ± 500	69083 ± 573
10	47729 ± 413	214808 ± 506	33607 ± 518	217156 ± 490	46822 ± 528	231903 ± 501	72371 ± 572
12	48713 ± 417	213524 ± 508	35555 ± 510	215942 ± 492	47525 ± 531	231376 ± 500	72803 ± 576

[a]Average values for all combinations of blocks for a given thickness. All measurements were for 1000 sec live time for the multichannel analyzer.

[b]Zero counts observed for A blocks baked.

Table D6. Individual boron capture gamma ray measurements results for baked BoroBond™ blocks

Block number	Nominal thickness (in.)	Integral counts for block series[a]		
		B	C	D
6	2	7724 ± 435	13260 ± 425	22429 ± 456
8	2	7374 ± 427	12160 ± 428	21181 ± 452
2	4	19140 ± 482	29718 ± 486	49348 ± 529
4	4	19029 ± 481	29881 ± 489	49523 ± 524
6,8	6	18386 ± 485	31459 ± 486	48486 ± 528
2,6	6	29095 ± 503	40391 ± 515	64500 ± 559
2,4	8	32999 ± 509	45350 ± 524	69083 ± 573
2,4,6	10	33607 ± 518	46822 ± 528	72371 ± 572
2,4,6,8	12	35555 ± 516	47525 ± 531	72803 ± 576

[a]Integral between 465 and 490 keV.